Article

Viruses inhibit TIR gcADPR signalling to overcome bacterial defence

https://doi.org/10.1038/s41586-022-05375-9

Received: 16 March 2022

Accepted: 21 September 2022

Published online: 29 September 2022

Check for updates

Azita Leavitt[1,6], Erez Yirmiya[1,6], Gil Amitai[1,6], Allen Lu[2,3,6], Jeremy Garb[1], Ehud Herbst[1], Benjamin R. Morehouse[2,3], Samuel J. Hobbs[2,3], Sadie P. Antine[2,3], Zhen-Yu J. Sun[4], Philip J. Kranzusch[2,3,5]✉ & Rotem Sorek[1]✉

The Toll/interleukin-1 receptor (TIR) domain is a key component of immune receptors that identify pathogen invasion in bacteria, plants and animals[1–3]. In the bacterial antiphage system Thoeris, as well as in plants, recognition of infection stimulates TIR domains to produce an immune signalling molecule whose molecular structure remains elusive. This molecule binds and activates the Thoeris immune effector, which then executes the immune function[1]. We identified a large family of phage-encoded proteins, denoted here as Thoeris anti-defence 1 (Tad1), that inhibit Thoeris immunity. We found that Tad1 proteins are 'sponges' that bind and sequester the immune signalling molecule produced by TIR-domain proteins, thus decoupling phage sensing from immune effector activation and rendering Thoeris inactive. Tad1 can also efficiently sequester molecules derived from a plant TIR-domain protein, and a high-resolution crystal structure of Tad1 bound to a plant-derived molecule showed a unique chemical structure of 1′′–2′ glycocyclic ADPR (gcADPR). Our data furthermore suggest that Thoeris TIR proteins produce a closely related molecule, 1′′–3′ gcADPR, which activates ThsA an order of magnitude more efficiently than the plant-derived 1′′–2′ gcADPR. Our results define the chemical structure of a central immune signalling molecule and show a new mode of action by which pathogens can suppress host immunity.

Toll/interleukin-1 receptor (TIR) domains serve as the signal-transducing modules in immune receptors that recognize pathogen invasion in the immune systems of bacteria, plants and animals[1–3]. Whereas TIR domains in animals mainly transfer the signal by protein–protein interactions[3], in bacteria and in some plants these domains produce an immune signalling molecule that has the same mass as cyclic ADP-ribose (cADPR)[1,4,5]. The mechanism of action of TIR-mediated immune signalling was recently deciphered for a bacterial antiphage immune system called Thoeris[1]. This system comprises two core proteins, one of which (named ThsB) has a TIR domain and serves as the sensor for phage infection. Recognition of phage triggers the ThsB TIR domain to produce the cADPR isomer molecule, and this molecule activates a second Thoeris protein, ThsA, which then depletes the cell of the essential molecule nicotinamide adenine dinucleotide (NAD^+) and leads to premature cell death that aborts infection[1,6]. Intriguingly, activation of plant TIRs by pathogens also leads to cell suicide that prevents pathogen propagation, and it was suggested that the cADPR isomer produced by TIRs is involved in mediation of this plant immune response[4,5,7].

Phage genes that inhibit Thoeris

We have isolated and analysed a group of closely related phages that infect *Bacillus subtilis*. This group includes eight phages similar to phage SBSphiJ, a Myoviridae phage with a genome roughly 150 kb in length[8]. Despite high sequence similarity between these phages, each had several genes not found in the genomes of other phages in the group (Extended Data Fig. 1 and Supplementary Table 1). The Thoeris defence system protected against all phages from the SBSphiJ group except for phage SBSphiJ7 (Fig. 1a). We therefore hypothesized that one or more genes that are unique to SBSphiJ7 allow this phage to escape or inhibit the activity of Thoeris.

To test this hypothesis we cloned five genes unique to phage SBSphiJ7, under the control of an inducible promoter, into *B. subtilis* cells that also express the Thoeris system from *Bacillus cereus* MSX-D12 (Supplementary Table 2). One of these genes, which we denote *tad1* (Thoeris anti-defence 1), robustly inhibited the activity of Thoeris, as phages that are normally blocked by Thoeris were able to infect Thoeris-expressing cells if these cells also expressed Tad1 (Fig. 1a,b). Silencing the expression of Tad1 in SBSphiJ7 using dCas9 (ref. [9]) caused SBSphiJ7 to be blocked by Thoeris, verifying that *tad1* is the gene responsible for the Thoeris-inhibiting phenotype of SBSphiJ7 (Fig. 1c). Moreover, knock-in of *tad1* into phage SBSphiJ, which does not naturally encode this gene, rendered the phage fully resistant to Thoeris, showing that *tad1* alone confers the anti-Thoeris phenotype (Fig. 1a).

Tad1 is a small protein (142 amino acids) of unknown function, with no recognizable protein domains. A search based on sequence

[1]Department of Molecular Genetics, Weizmann Institute of Science, Rehovot, Israel. [2]Department of Microbiology, Harvard Medical School, Boston, MA, USA. [3]Department of Cancer Immunology and Virology, Dana-Farber Cancer Institute, Boston, MA, USA. [4]Department of Cancer Biology, Dana-Farber Cancer Institute, Boston, MA, USA. [5]Parker Institute for Cancer Immunotherapy at Dana-Farber Cancer Institute, Boston, MA, USA. [6]These authors contributed equally: Azita Leavitt, Erez Yirmiya, Gil Amitai, Allen Lu. ✉e-mail: philip_kranzusch@dfci.harvard.edu; rotem.sorek@weizmann.ac.il

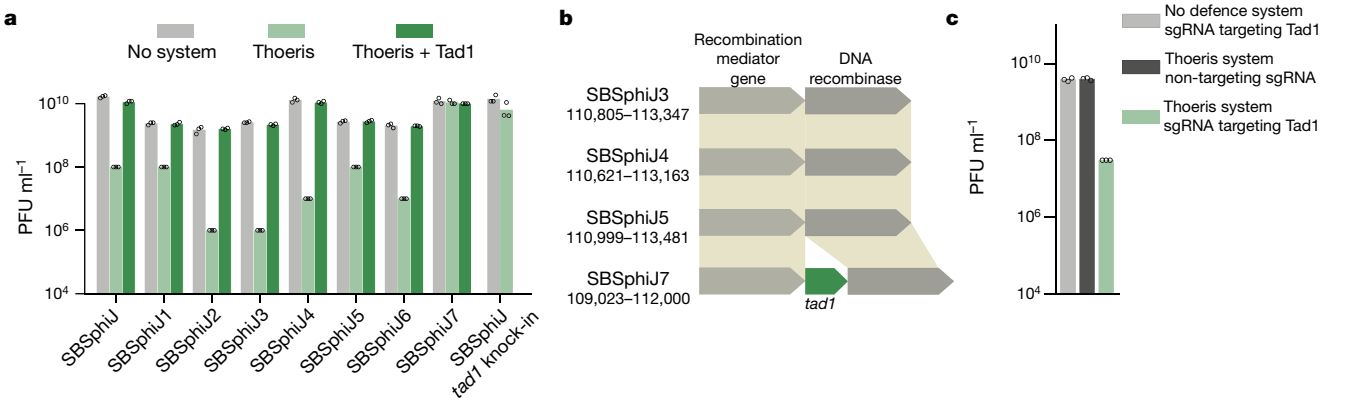

Fig. 1 | Tad1 inhibits Thoeris defence. a, Differential defence of Thoeris against SBSphiJ phages, and anti-Thoeris activity of Tad1. Data represent plaque-forming units per millilitre (PFU ml^{-1}) of phages infecting control cells (no system), cells expressing the Thoeris system (Thoeris) and cells co-expressing the T hoeris system and the *tad1* gene from SBSphiJ7 (Thoeris + Tad1). All phages except for SBSphiJ7 naturally lack *tad1*. Data for phage SBSphiJ, in which *tad1* was engineered under the control of its native promoter, are also presented. Shown is the average of three replicates, with individual data points overlaid. **b**, The *tad1* locus in SBSphiJ7, shown in the locus for three other phages, SBSphiJ3, SBSphiJ4 and SBSphiJ5, in which *tad1* is absent. The coordinates of the presented locus within the phage genome are indicated below the name of each phage. **c**, Tad1 knockdown cancels anti-Thoeris activity. Data represent PFU ml^{-1} of SBSphiJ7 that infects cells expressing Thoeris and a dCas9 system targeting Tad1, as well as control cells. Shown is the average of three replicates, with individual data points overlaid. sgRNA, single-guide RNA.

homology identified 799 Tad1 homologues in the databases Integrated Microbial Genomes (IMG)[10] and Metagenomic Gut Virus (MGV)[11] (Supplementary Tables 3 and 4). Strikingly, all homologues of Tad1 reside either in phage genomes or in genomes of prophages integrated within bacterial genomes, indicating that this protein primarily executes a phage function. Tad1-encoding phages belong to multiple phage families, including Myoviridae, Podoviridae and Siphoviridae, and infect at least 60 species of bacteria from a diverse set of taxonomic phyla including Proteobacteria, Firmicutes and Cyanobacteria (Fig. 2a and Supplementary Tables 3 and 4).

Phylogenetic analysis showed that Tad1 proteins can be divided into four major clades (Fig. 2a). In some cases, phages encoding Tad1 proteins from the same phylogenetic clade belonged to different phage families, suggesting that *tad1* genes can be horizontally transferred between phages (Fig. 2a). We selected ten Tad1 homologues that span the phylogenetic diversity of the Tad1 family and cloned each of them into *B. subtilis* cells expressing the Thoeris system (Fig. 2a and Extended Data Fig. 2). All ten Tad1 family proteins were able to inhibit Thoeris, including homologues derived from phages that infect distant organisms such as *Leptolyngbya* sp., *Opitutaceae* sp. and *Acinetobacter baumannii* (Fig. 2). Together, these results reveal a large family of proteins utilized by phages to inhibit the activity of the Thoeris bacterial defence system.

Tad1 sequesters TIR-derived molecules

The hallmark of Thoeris defence is the TIR-domain ThsB protein which, after sensing infection, produces a signalling molecule that triggers the NADase activity of the Thoeris ThsA protein[1]. To test whether this signalling molecule is produced in the presence of Tad1, we experimented with cells expressing a Thoeris system in which ThsA was mutated in its NADase active site such that only ThsB is active. We infected these cells with phage SBSphiJ that naturally lacks Tad1, and then lysed the cells and filtered the lysates to enrich for molecules smaller than 3 kDa (Fig. 3a). As expected, purified ThsA protein incubated with these filtered lysates in vitro showed strong NADase activity, indicating that the TIR-domain ThsB protein produced the signalling molecule within the cell in response to SBSphiJ infection (Fig. 3b). However, filtered lysates derived from cells in which Tad1 was co-expressed with ThsB, or from cells infected by SBSphiJ7 that naturally encodes Tad1, failed to activate ThsA in vitro, suggesting that the signalling molecule was eliminated or inactivated in Thoeris-infected cells that co-express Tad1 (Fig. 3b and Extended Data Fig. 3). Liquid chromatography followed by mass spectrometry (LC–MS) confirmed that the signalling molecule, having a mass identical to that of cADPR, was present in lysates of infected cells expressing the TIR-domain protein ThsB but absent in lysates derived from infected cells in which ThsB was co-expressed with Tad1 (Fig. 3c). These results indicate that Tad1 does not inhibit the Thoeris effector protein ThsA, but rather inhibits Thoeris upstream of ThsA.

We next experimented with a purified Tad1 homologue from a prophage integrated in *Clostridioides mangenotii* (cmTad1), which showed high stability when purified in vitro. To test whether cmTad1 could directly eliminate the signalling molecule from the lysate, we collected filtered lysates from cells overexpressing ThsB that were infected by phage SBSphiJ and incubated these lysates with cmTad1 for 10 min (Fig. 3d). Lysates incubated with purified cmTad1 completely lost the ability to induce the NADase activity of ThsA, demonstrating that Tad1 rapidly eliminates the signalling molecule from the filtered lysate rather than inhibiting its production (Fig. 3e).

Some phages were previously shown to inhibit bacterial immune signalling—for example, cyclic oligoadenylate signalling in type III CRISPR–Cas and CBASS systems, by introducing enzymes that cleave the signalling molecules[12,13]. We therefore presumed that Tad1 is an enzyme that cleaves the immune molecule of Thoeris. Under this hypothesis, one would expect Tad1 to deplete the signalling molecule in a time-dependent manner. However, counter to our hypothesis, incubation of subinhibitory concentrations of cmTad1 with the filtered lysate for prolonged periods did not result in time-dependent increased depletion of the active molecule from the lysate (Fig. 3f). These results implied that Tad1 is not an enzyme, but rather a 'sponge' that binds and sequesters the signalling cADPR isomer molecule.

To further examine the hypothesis that Tad1 tightly binds the cADPR isomer signalling molecule, we tested whether cmTad1 denaturation could release the bound molecule into the buffer. For this, we first incubated cmTad1 with the signal-containing lysate for 10 min and then denatured it by exposure to 85 °C for 5 min. We found that, following Tad1 denaturation, the buffer regained the capacity to activate ThsA in vitro (Fig. 3g). These results demonstrate that Tad1 binds and sequesters, but does not degrade, the Thoeris signalling molecule and that denaturation of Tad1 releases the bound molecule intact. Our results therefore show that Tad1 inhibits Thoeris defence by physically binding and sequestering the ThsB-derived signalling molecule, thus

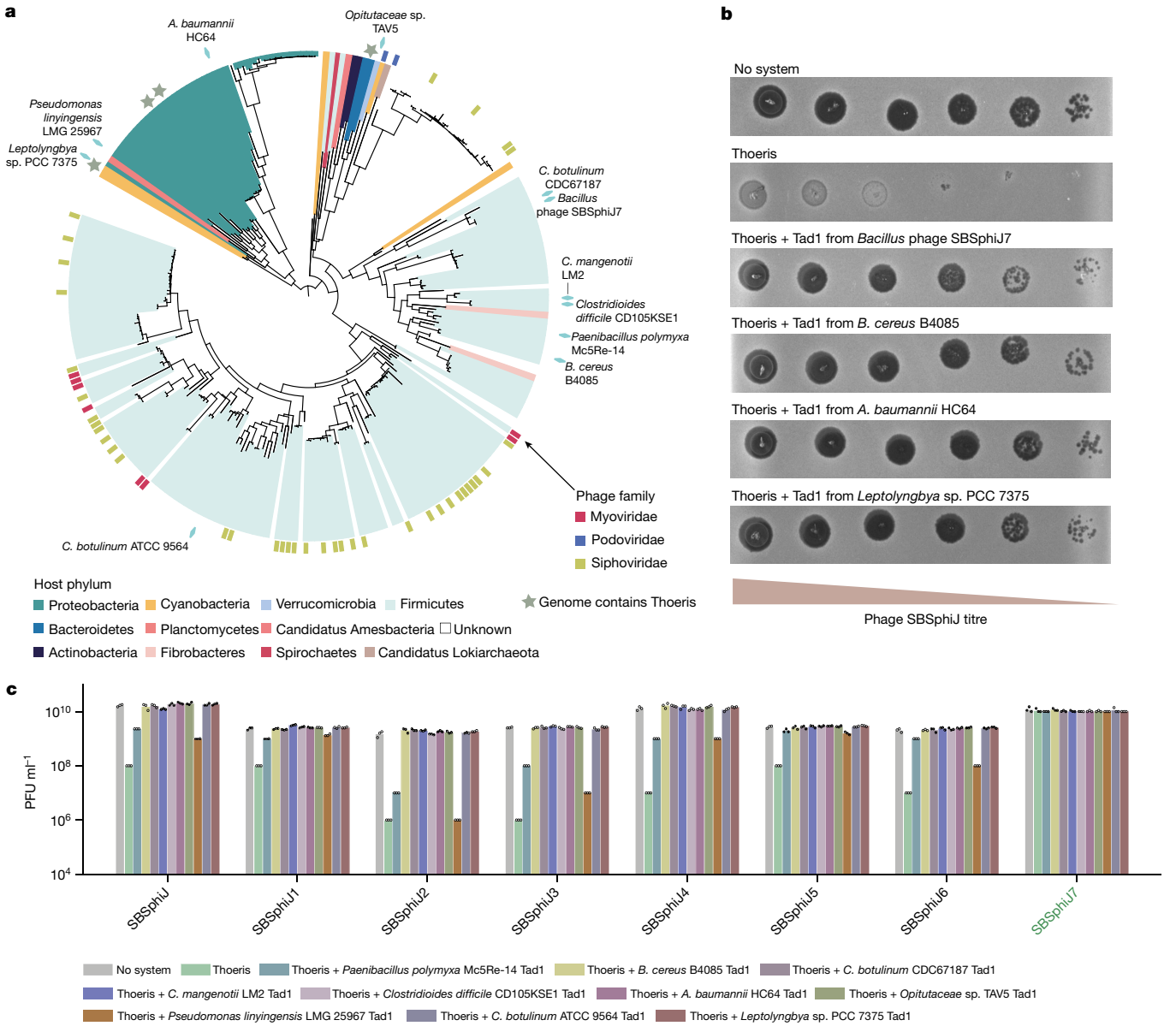

Fig. 2 | Tad1 proteins inhibit Thoeris defence. a, Phylogenetic analysis of Tad1 homologues in phage and prophage genomes. The names of bacteria in which Tad1 homologues were found in prophages and tested experimentally are indicated on the tree by cyan diamonds. The tree is based on 256 non-redundant sequences. **b**, Tad1 homologues inhibit the Thoeris system in *B. subtilis*. Shown are tenfold serial dilution plaque assays with phage SBSphiJ. **c**, Results of phage infection experiments with eight phages of the SBSphiJ family. Data represent PFU ml^{-1} of phages infecting control cells without Thoeris, cells expressing the Thoeris system and cells co-expressing the Thoeris system and a Tad1 homologue. All phages except for SBSphiJ7 lack Tad1. Shown is the average of three replicates, with individual data points overlaid. The 'Thoeris' and 'no system' data presented here are the same as those presented in Fig. 1a.

preventing activation of the Thoeris immune effector and mitigating Thoeris-mediated defence.

It was previously shown that cADPR isomer molecules produced by plant TIR proteins can activate the Thoeris effector ThsA[1]. We therefore co-expressed cmTad1 with a TIR-domain protein from the plant *Brachypodium distachyon* (BdTIR), which was shown to constitutively produce a ThsA-activating cADPR isomer molecule when expressed in *Escherichia coli*[1,4] (Extended Data Fig. 4a,b). cmTad1 purified from BdTIR-expressing cells showed a substantial shift during size-exclusion chromatography and exhibited increased absorption at UV_{260} as compared with cmTad1 purified from control cells, suggesting that cmTad1 binds the cADPR isomer molecule produced by the plant TIR (Extended Data Fig. 4c,d). Consistent with this observation, in vitro addition of purified cmTad1 to lysates derived from BdTIR-expressing cells eliminated a specific molecule as observed from high-performance LC (HPLC) analysis, further supporting the premise that cmTad1 binds the BdTIR-derived molecule (Extended Data Fig. 4a,b). Furthermore, supernatant collected from heat denaturation of the molecule-bound cmTad1 was able to activate ThsA, verifying that the cADPR isomer molecule produced by the plant TIR, which was bound by cmTad1 and migrated uniquely on HPLC, is able to activate the Thoeris system (Extended Data Fig. 4a,b,e). We found that the BdTIR-derived molecule binds cmTad1 with $K_D = 241 \pm 22$ nM (Extended Data Fig. 4f).

Structure of Tad1 bound to glycocyclic ADPR signal

To define the molecular mechanism of Tad1 anti-Thoeris evasion, we next determined crystal structures of Tad1 from a *Clostridium botulinum*

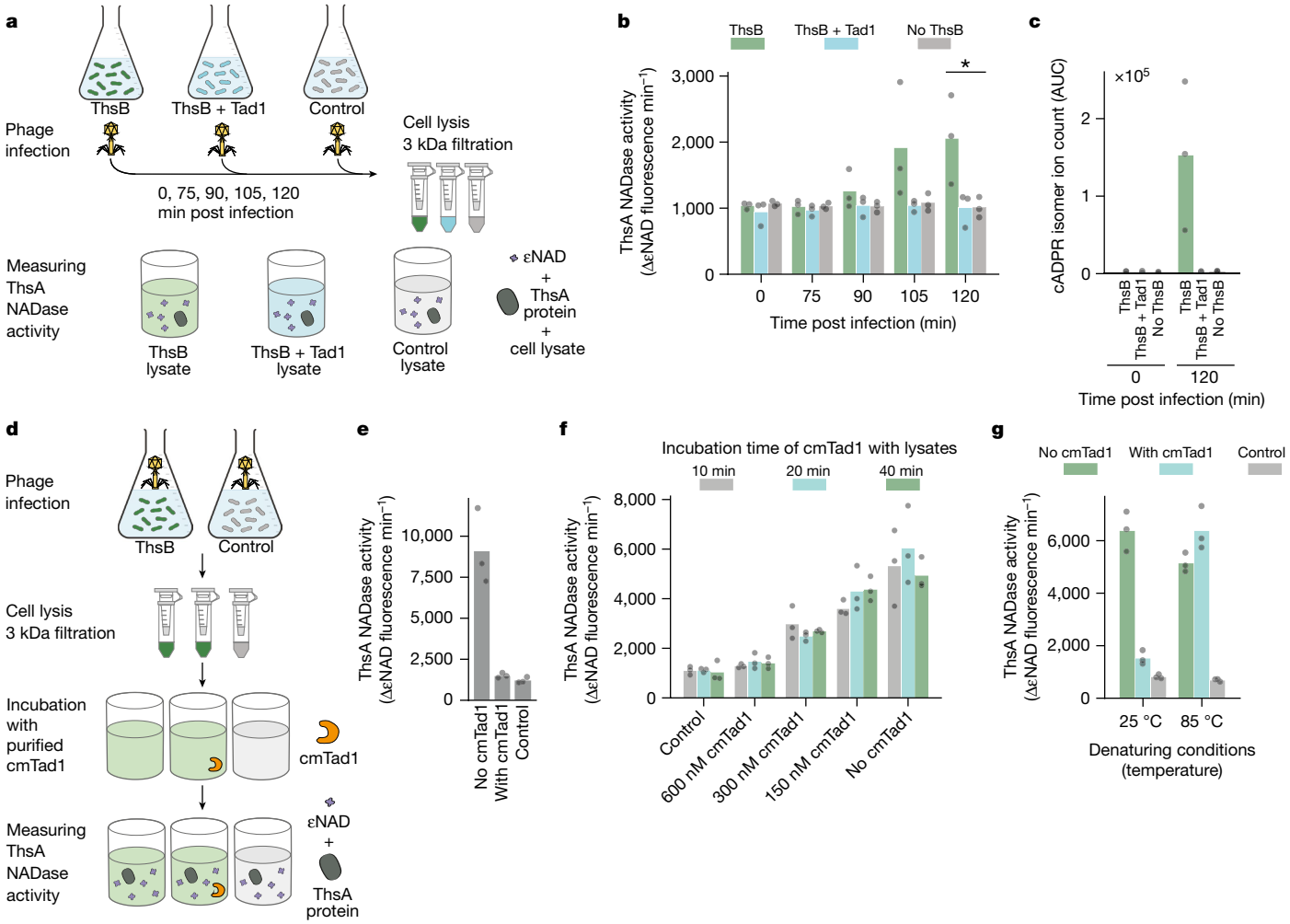

Fig. 3 | Tad1 cancels Thoeris-mediated defence by physically binding and sequestering the Thoeris-derived signalling molecule. a, Schematic representation of the ThsB/Tad1 co-expression experiment. Cells expressing ThsB (native promoter), both ThsB (native promoter) and Tad1 (induced by 1 mM isopropyl-ß-D-thiogalactopyranoside (IPTG)) or control cells that do not express ThsB were infected with phage SBSphiJ at a multiplicity of infection (MOI) of 5. NADase activity of purified ThsA incubated with filtered lysates was measured using a nicotinamide 1,N6-ethenoadenine dinucleotide (εNAD) cleavage fluorescence assay. **b**, Activation of ThsA NADase activity by lysates from infected cells. Bars represent the mean of three experiments, with individual data points overlaid. Asterisk denotes a statistically significant difference in NADase activity (one-way analysis of variance, $P = 0.036$). **c**, Co-expression of Tad1 with ThsB eliminates the signalling molecule normally produced by ThsB in infected cells. Lysates derived from infected cells were analysed by LC–MS. The *y* axis represents the area under the curve (AUC) of cADPR isomer ions detected in MS analysis. Time 0 represents uninfected cells. **d**, Schematic representation of the Tad1/lysate incubation experiment. Cells overexpressing ThsB (0.1 mM IPTG) or control cells not expressing ThsB were infected with phage SBSphiJ at a MOI of 5 at 25 °C. After 120 min the cells were lysed and lysates filtered, then incubated with purified cmTad1. ThsA was added to the lysates and the NADase activity of ThsA was measured. **e**, Purified Tad1 eliminates the signalling molecule from infected lysates. Filtered lysates were preincubated either with 600 nM purified cmTad1 for 10 min in vitro (with cmTad1) or with buffer (no cmTad1). **f**, Tad1 is not an enzyme. Filtered lysates were incubated in vitro for 10, 20 or 40 min with either purified cmTad1 or buffer before exposure to ThsA. **g**, Tad1 releases bound molecules when denatured. Shown is the NADase activity of purified ThsA incubated with filtered lysates derived from infected cells overexpressing ThsB and that were additionally preincubated with purified cmTad1 in vitro for 10 min, followed by an additional incubation of 5 min at either 25 or 85 °C (denaturing conditions). 'With cmTad1', lysates preincubated with cmTad1; 'no cmTad1', lysates incubated with buffer rather than cmTad1. Control is lysates derived from infected cells that do not express ThsB.

prophage (cbTad1) in the apo and ligand-bound states (Extended Data Table 1). The structure of Tad1 shows a homodimeric complex with two protomers arranged head to tail (Fig. 4a). Each protomer forms an N-terminal antiparallel β-sheet (β1–β4) and two long C-terminal helices (α1 and α2) that create a wedge-shaped architecture and allow tight interlocking of $Tad1_a$ and $Tad1_b$ into a compact assembly (Fig. 4a,b). The N-terminal β-sheets join through a $\beta4_a$–$\beta4_b$ hydrophilic seam to form the front face of the Tad1 assembly, whereas the C-terminal helices align to create a four-helix bundle that seals the back face (Fig. 4a,b). The tightly locked assembly creates two recessed ligand-binding pockets at the top and bottom ends of the Tad1 complex, each surrounded by four highly conserved loops within β2–β3, β4–α1 and the C-terminal tail of $Tad1_a$, along with α1–α2 donated by the partner protomer $Tad1_b$ (Fig. 4b and Extended Data Fig. 2).

Following binding to the plant BdTIR-derived molecule, the Tad1 complex undergoes rotation of 3° to close and envelope the signalling molecule. Tad1 loop β4–α1 moves by about 3.5 Å and C-terminal residues 116–122 form an ordered lid that together seal the ligand-binding site (Fig. 4c). Exceptionally clear density within the 1.9 Å ligand-bound cbTad1 complex allowed for unambiguous assignment of each atomic position within the BdTIR-derived signalling molecule, showing the compound 1′′–2′ glycosyl cyclic adenosine diphosphate ribose (1′′–2′

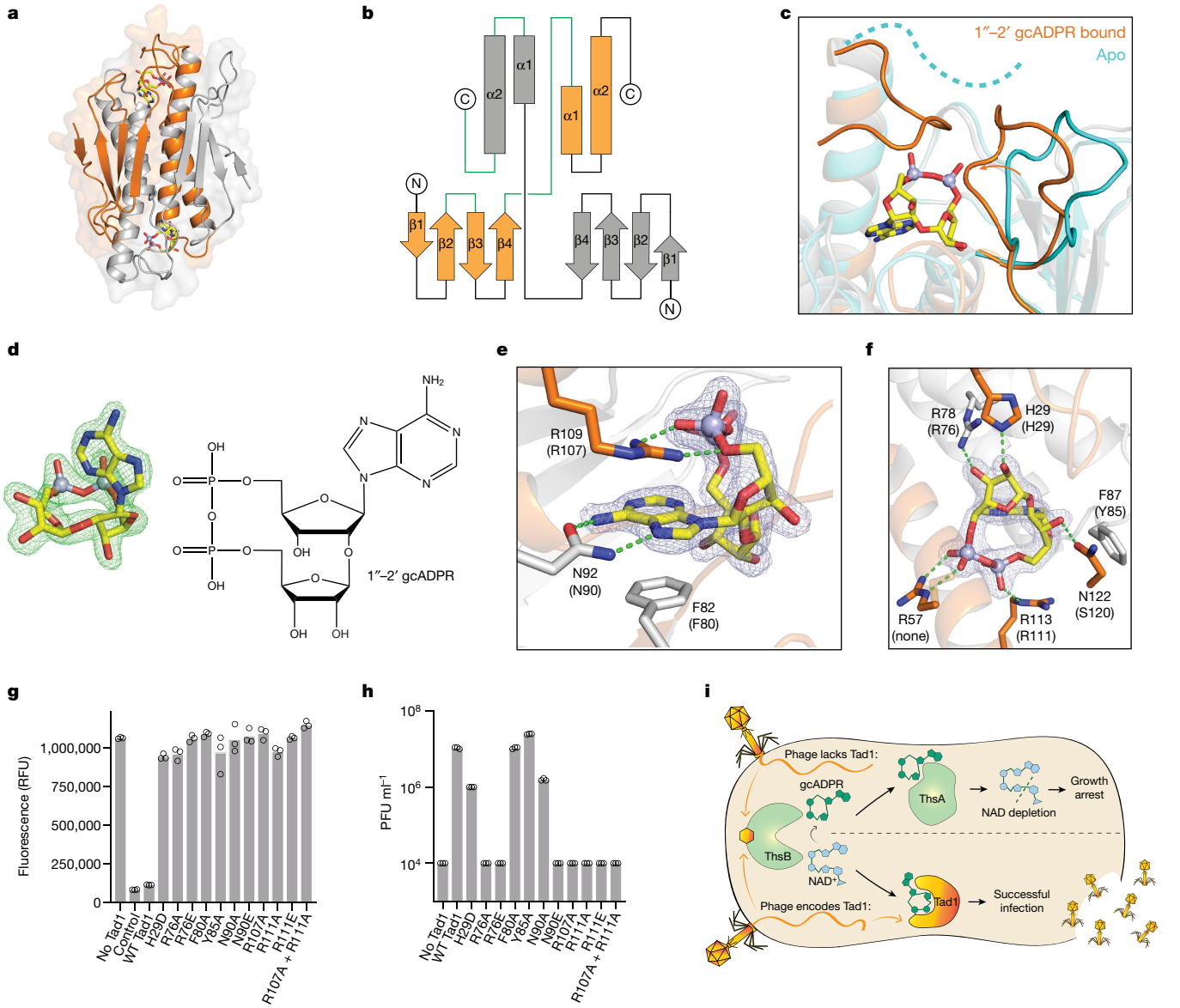

Fig. 4 | Structure of Tad1 and identification of 1″–2′ gcADPR. a, Overview of the cbTad1 crystal structure in front view bound to BdTIR-derived 1″–2′ glycocyclic ADPR (gcADPR; yellow). Tad1 forms a homodimer with two ligand-binding sites, with one monomer shown in orange and the other in grey. **b**, Topology map of Tad1 from a top view perspective. Loops that form one binding site are highlighted in green. **c**, Comparison of the ligand-binding site of cbTad1 in the apo state (cyan) and in complex with 1″–2′ gcADPR (orange and grey). Following ligand binding, cbTad1 loop β4–α1 shifts by around 3.7 Å (measured by A56 amine movement) and the C-terminal tail becomes structured to enclose around the molecule. **d**, Polder omit map of the Tad1 ligand-binding site contoured at 6σ shows the chemical structure of the ligand as 1″–2′ gcADPR. **e**,**f**, Detailed views of cbTad1 residues interacting with the adenine base of 1″–2′ gcADPR (**e**) or with ribose moieties and phosphates (**f**). Conserved residues in cmTad1 are labelled separately in parentheses. Separate monomer chains are shown in either orange or grey. Green dashed lines denote hydrogen bonding interactions. Light blue mesh denotes 1″–2′ gcADPR $2F_o - F_c$ electron density contoured at 1.8σ. **g**, Tad1 mutations abolish 1″–2′ gcADPR binding in vitro. Wild-type (WT) and mutated cmTad1 were incubated with 1″–2′ gcADPR; the reactions were then filtered and their ability to activate ThsA NADase activity was measured. Bars represent the mean of three experiments, with individual data points overlaid. Control reaction contained buffer with no 1″–2′ gcADPR. **h**, Tad1 mutations result in loss of anti-defence activity. Data represent PFU ml^{-1} of phage SBSphiJ2 infecting cells co-expressing Thoeris and WT or mutated cmTad1. Shown is the average of three replicates, with individual data points overlaid. **i**, Model of the mechanism of Tad1. RFU, relative fluorescence units.

gcADPR) (Fig. 4d). In contrast to the canonical cADPR, in which cyclization occurs through the ribose and the N1 position in the adenine nucleobase, our data demonstrate that the molecule produced by the plant BdTIR protein is unexpectedly cyclized through a unique ribose–ribose glycosidic bond. The Tad1 ligand-binding pocket intimately embraces 1″–2′ gcADPR with 11 residues forming base- and linkage-specific contacts (Fig. 4e,f). The 1″–2′ gcADPR adenine base is stacked between cbTad1 F82 and R109, with N92 making sequence-specific contacts with the Hoogsteen edge (Fig. 4e). The diphosphate backbone is bound by three cbTad1 sidechains, R57, R109 and R113, and additional peptide-backbone contacts from R57 and G120. Finally, cbTad1 F87 buttresses the adenosine ribose and residues H29, G55(NH), R78 and N122 coordinate each free OH in the ribose–ribose linkage, explaining the intimate binding capabilities of Tad1 for this linkage in 1″–2′ gcADPR (Fig. 4f). Complete enclosure within the ligand-binding pocket explains how Tad1 efficiently binds and sequesters the BdTIR-derived signal. Mutations in the corresponding adenine- and diphosphate-binding residues in cmTad1 resulted in loss of binding capacity to 1″–2′ gcADPR

in vitro (Fig. 4g), with the majority of these mutants also resulting in partial or full loss of Tad1 anti-defence activity in vivo (Fig. 4h).

Nuclear magnetic resonance (NMR) analysis confirmed the molecular structure of the BdTIR-derived molecule to be ″–2′ gcADPR (Extended Data Fig. 5 and Extended Data Table 2). We next purified the cADPR isomer produced from in vitro reactions performed with a ThsB TIR-domain protein. Interestingly, the ThsB-derived cADPR isomer signal exhibited distinct migration on HPLC and more potently activated ThsA compared with the plant-derived 1″–2′ gcADPR molecule, suggesting that the Thoeris system produces a different cADPR isomer (Extended Data Fig. 6).

Recent studies have shown that the TIR domain of AaTIR, a protein of unknown function from the organism *Aquimarina amphilecti*, generates a 1″–3′ gcADPR product in vitro[14,15]. We found that AaTIR-derived 1″–3′ gcADPR (Extended Data Fig. 7) shows a signal matching the molecule derived from Thoeris ThsB on HPLC, suggesting that the active molecule in the Thoeris system is 1″–3′ gcADPR (Extended Data Fig. 7d,e). The Thoeris molecule 1″–3′ gcADPR is an isomer of 1″–2′ gcADPR, in which the ribose–ribose glycosyl bond occurs on the 3′ carbon position of the adenine ribose. This molecule was able to activate the NADase activity of ThsA an order of magnitude more potently than 1″–2′ gcADPR, further supporting the concept that 1″–3′ gcADPR is the molecule naturally produced by Thoeris (Extended Data Fig. 6e,f). Tad1 binds and sequesters both 1″–2′ gcADPR (Extended Data Fig. 4) and 1″–3′ gcADPR (Extended Data Fig. 7), demonstrating that Tad1 is capable of sequestering multiple isoforms of gcADPR to block immune activation.

Together, our data show a complete mechanism of viral subversion from TIR-derived signalling through signal molecule sequestration (Fig. 4i). We envision that similar mechanisms may be employed by plant pathogens to inhibit TIR-mediated plant immunity, and that signal sequestration could be a general mechanism utilized by viruses to evade immune responses that rely on signalling molecules. Our results establish gcADPR family molecules as signalling molecules produced by bacterial and plant TIR proteins. Although the contribution of BdTIR to *B. distachyon* immunity remains unclear[4], recent studies intriguingly show that other plant immune TIR proteins can produce a variety of immune signalling molecules, including 2′,3′-cAMP/cGMP[16], 2′-(5″-phosphoribosyl)–5′-adenosine mono-/diphosphate[17] and ATP–ADPR conjugates[18]. Some of these molecules were shown to bind and activate plant protein complexes that contain EDS1, which is known as essential for promotion of plant cell death in response to pathogen recognition by plant TIRs[16–18]. Therefore, as in other immune pathways that employ signalling molecules[19–21], TIR-centric pathways can produce a diversity of related immune signals[22]. Finally, because recent studies exposed numerous antiviral mechanisms that are conserved from bacteria to humans[21,23–25], it would be intriguing to examine whether the human immune system also involves gcADPR signalling.

Online content

Any methods, additional references, Nature Research reporting summaries, source data, extended data, supplementary information, acknowledgements, peer review information; details of author contributions and competing interests; and statements of data and code availability are available at https://doi.org/10.1038/s41586-022-05375-9.

1. Ofir, G. et al. Antiviral activity of bacterial TIR domains via immune signalling molecules. *Nature* **600**, 116–120 (2021).
2. Burch-Smith, T. M. & Dinesh-Kumar, S. P. The functions of plant TIR domains. *Sci. STKE* **2007**, pe46 (2007).
3. Fitzgerald, K. A. & Kagan, J. C. Toll-like receptors and the control of immunity. *Cell* **180**, 1044–1066 (2020).
4. Wan, L. et al. TIR domains of plant immune receptors are NAD^+-cleaving enzymes that promote cell death. *Science* **365**, 799–803 (2019).
5. Horsefield, S. et al. NAD^+ cleavage activity by animal and plant TIR domains in cell death pathways. *Science* **365**, 793–799 (2019).
6. Ka, D., Oh, H., Park, E., Kim, J.-H. & Bae, E. Structural and functional evidence of bacterial antiphage protection by Thoeris defense system via NAD^+ degradation. *Nat. Commun.* **11**, 2816 (2020).
7. Bayless, A. M. & Nishimura, M. T. Enzymatic functions for Toll/interleukin-1 receptor domain proteins in the plant immune system. *Front. Genet.* **11**, 539 (2020).
8. Doron, S. et al. Systematic discovery of antiphage defense systems in the microbial pangenome. *Science* **359**, eaar4120 (2018).
9. Peters, J. M. et al. A comprehensive, CRISPR-based functional analysis of essential genes in bacteria. *Cell* **165**, 1493–1506 (2016).
10. Chen, I. M. A. et al. IMG/M v.5.0: an integrated data management and comparative analysis system for microbial genomes and microbiomes. *Nucleic Acids Res.* **47**, D666–D677 (2019).
11. Nayfach, S. et al. Metagenomic compendium of 189,680 DNA viruses from the human gut microbiome. *Nat. Microbiol.* **6**, 960–970 (2021).
12. Athukoralage, J. S. et al. An anti-CRISPR viral ring nuclease subverts type III CRISPR immunity. *Nature* **577**, 572–575 (2020).
13. Hobbs, S. J. et al. Phage anti-CBASS and anti-Pycsar nucleases subvert bacterial immunity. *Nature* **605**, 522–526 (2022).
14. Manik, M. K. et al. Cyclic ADP ribose isomers: Production, chemical structures, and immune signaling. *Science* **377**, eadc8969 (2022).
15. Weagley, J. S. et al. Products of gut microbial Toll/interleukin-1 receptor domain NADase activities in gnotobiotic mice and Bangladeshi children with malnutrition. *Cell Rep.* **39**, 110738 (2022).
16. Yu, D. et al. TIR domains of plant immune receptors are 2′,3′-cAMP/cGMP synthetases mediating cell death. *Cell* **185**, 2370–2386 (2022).
17. Huang, S. et al. Identification and receptor mechanism of TIR-catalyzed small molecules in plant immunity. *Science* **377**, eabq3297 (2022).
18. Jia, A. et al. TIR-catalyzed ADP-ribosylation reactions produce signaling molecules for plant immunity. *Science* **377**, eabq8180 (2022).
19. Tal, N. et al. Cyclic CMP and cyclic UMP mediate bacterial immunity against phages. *Cell* **184**, 5728–5739 (2021).
20. Whiteley, A. T. et al. Bacterial cGAS-like enzymes synthesize diverse nucleotide signals. *Nature* **567**, 194–199 (2019).
21. Cohen, D. et al. Cyclic GMP-AMP signalling protects bacteria against viral infection. *Nature* **574**, 691–695 (2019).
22. Essuman, K., Milbrandt, J., Dangl, J. L. & Nishimura, M. T. Shared TIR enzymatic functions regulate cell death and immunity across the tree of life. *Science* **377**, eabo0001 (2022).
23. Johnson, A. G. et al. Bacterial gasdermins reveal an ancient mechanism of cell death. *Science* **375**, 221–225 (2022).
24. Bernheim, A. et al. Prokaryotic viperins produce diverse antiviral molecules. *Nature* **589**, 120–124 (2021).
25. Morehouse, B. R. et al. STING cyclic dinucleotide sensing originated in bacteria. *Nature* **586**, 429–433 (2020).

Methods

Phage strains, isolation, cultivation and sequencing

Phage SBSphiJ was isolated in a previous study[8]. Other phages used in this study were isolated from soil samples on *B. subtilis* BEST7003 culture as described in Doron et al.[8]. For this, soil samples were added to a log-phase *B. subtilis* BEST7003 culture and incubated overnight to enrich for *B. subtilis* phages. The enriched samples were centrifuged and filtered through 0.45 µm filters, and the filtered supernatant was used to perform double-layer plaque assays as described in Kropinski et al.[26]. Single plaques that appeared after overnight incubation were picked, reisolated three times and amplified as described below.

Phages were propagated by picking a single phage plaque into a liquid culture of *B. subtilis* BEST7003 grown at 37 °C to an optical density (OD_{600}) of 0.3 in magnesium manganese broth (MMB) (lysogeny broth, 0.1 mM $MnCl_2$ and 5 mM $MgCl_2$) until culture collapse. The culture was then centrifuged for 10 min at 3,200*g* and the supernatant filtered through a 0.2 µm filter to remove remaining bacteria and bacterial debris.

High-titre phage lysates (over 10^7 PFU ml^{-1}) were used for DNA extraction; 500 µl of the phage lysate was treated with the addition of DNase-I (Merck, no. 11284932001) to a final concentration of 20 mg ml^{-1} and incubated at 37 °C for 1 h to remove bacterial DNA. DNA was extracted using the QIAGEN DNeasy blood and tissue kit (no. 69504) starting from the Proteinase-K treatment step to lyse phages. Libraries were prepared for Illumina sequencing using a modified Nextera protocol as previously described[27].

Following Illumina sequencing, adaptor sequences were removed from the reads using Cutadapt v.2.8 (ref. [28]) with the option '-q 5'. The trimmed reads from each phage genome were assembled into scaffolds using SPAdes genome assembler v.3.14.0 (ref. [29]), with the '–careful' flag. Each assembled genome was analysed with Prodigal v.2.6.3 (ref. [30]) (default parameters) to predict open reading frames.

Plaque assays

Phage titre was determined using the small-drop plaque assay method[31]: 400 µl of bacterial culture was mixed with 30 ml of melted MMB 0.5% agar, poured on 10 cm square plates and left to dry for 1 h at room temperature. In cases of bacteria expressing anti-defence candidates, 1 mM IPTG was added to the medium. In cases of bacteria expressing dCas9–guide RNA constructs, 0.002% xylose was added to the medium. Tenfold serial dilutions in MMB were performed for each of the tested phages and drops of 10 µl were placed on the bacterial layer. After the drops had dried up, the plates were inverted and incubated at room temperature overnight. Plaque-forming units were determined by counting the derived plaques after overnight incubation, and lysate titre was determined by calculating PFU ml^{-1}. When no individual plaques could be identified, a faint lysis zone across the drop area was considered to be ten plaques. Efficiency of plating was measured by comparing plaque assay results for control bacteria and bacteria containing the defence system and/or a candidate anti-defence gene.

Prediction and cloning of candidate anti-Thoeris genes

Predicted protein sequences from all phage genomes were clustered into groups of homologues using the cluster module in MMSeqs2 release 12-113e3 (ref. [32]), with the parameters '-e 10', '-c 0.8', '-s 8' and '–min-seq-id 0.3' and the flag '–single-step-clustering'. Anti-Thoeris candidates were defined as clusters that included a single member derived from phage SBSphiJ7. The DNA of each anti-Thoeris candidate was amplified from the genome of phage SBSphiJ7 using KAPA HiFi HotStart ReadyMix (Roche, no. KK2601) with primers as indicated in Supplementary Table 2. Homologues of *tad1* were synthesized by Genscript Corp. Anti-Thoeris candidates were cloned into the pSG-*thrC*-Phspank vector (Supplementary File 1) and transformed to DH5α-competent cells. The cloned vector was subsequently transformed into *B. subtilis* BEST7003 cells containing the Thoeris defence system[8], resulting in cultures expressing both Thoeris and an anti-Thoeris gene candidate. As a negative control, a transformant with an identical plasmid containing green fluorescent protein in place of the anti-Thoeris gene was used. Transformation to *B. subtilis* was performed using MC medium as previously described[8]. Whole-genome sequencing was then applied to all transformed *B. subtilis* strains, and Breseq analysis[33] was used to verify the integrity of the inserts and absence of mutations.

Construction of dCas9 and gRNA cassette for integration with *B. subtilis thrC* site

A shuttle vector was constructed for the integration of dCas9 from *Streptococcus pyogenes* into the *thrC* gene of *B. subtilis*. The *dCas9* gene, including its xyl promoter and xylR, was amplified from pJMP1 (Addgene, plasmid no. 79873) using primers CTTCTAGGATCAAATCGATATCTCTGCAGTCGCG and AAAAATCCTTTTCTTTCTTATCTTGTGATTGGTGTATCATTTCGTTTTTCTTTTGTGC. The gRNA with a constitutive *B. subtilis* promoter was amplified from pJMP3 (Addgene, plasmid no. 79875) using primers AGATATCGATTTGATCCTAGAAGCT TATCGAATTCCTTATTAACGT and CGAATTCGACTCTCTAGCTCTAC CATCGGCGCTACGG. The two fragments were cloned into a backbone amplified from pSG_thrC_Phspank_sfGFP[34] using primers CAAGATAA GAAAGAAAAGGATTTTTCGCTACG and AGCTAGAGAGTCGAATTCG GATCCG, resulting in a plasmid named pJG_thrC_dCAS9_gRNA (Supplementary File 2).

To insert new spacers, two fragments were amplified from pJG_thrC_dCAS9_gRNA and the new spacer was introduced into the overlap of primers designed for NEBuilder HiFi DNA Assembly (NEB, no. E2621). For the gRNA used to target *tad1*, the first fragment was amplified using primers TTCAACAAACGAAAATTGGATAAAGTGGGAT and GAACCAC TACGAAATGATGGTTTTAGAGCTAGAAATAGCAAGTTAAAATAAGGCT, and the second using primers CCAATTTTCGTTTGTTGAACTAATGGGTG and CATCATTTCGTAGTGGTTCCACATTTATTGTACAACACGAGCCC ATTT. The resulting assembled construct had the gRNA sequence GGAACCACTACGAAATGAT.

The gRNA sequence CTATGATTGATTTTTTTAGC was used as a control. It was constructed as mentioned above, with primers TTCAACAAACGAAAATTGGATAAAGTGGGAT and TGTCTATGATT GATTTTTTTAGCGTTTTAGAGCTAGAAATAGCAAGTTAAAATAAGGCT, and CCAATTTTCGTTTGTTGAACTAATGGGTG and GCTAAAAAAAT CAATCATAGACATTTATTGTACAACACGAGCCCATTT. The resulting vectors containing the dCas9–gRNA sequences were cloned to a *B. subtilis* strain containing the Thoeris defence system, as well as to a control strain lacking Thoeris. Shuttle vectors were propagated in *E. coli* DH5a with 100 µg ml^{-1} ampicillin selection. Plasmids were isolated from *E. coli* DH5a before transformation into the appropriate *B. subtilis* BEST7003 strains.

Knock-in of *tad1* into phage SBSphiJ

The DNA sequence of *tad1*, together with its upstream intergenic region, was amplified from the genome of phage SBSphiJ7 using KAPA HiFi HotStart ReadyMix (Roche, no. KK2601) with the primer pair CAACTGAGTAAATAAATAGAGCCTAGTGTAACGAC and CTTTGCCAAGTGTTTTCCCTCCA. The upstream and downstream genomic arms (±1.2 kbp) for the integration site of the *tad1* insert within the SBSphiJ genome were amplified from the genome of phage SBSphiJ using the primer pair ACTCTTGTTAACTCTAGAGCT ATGTCATTCTTAGACATTGTAAACCAAGAAGCAG and GGCTCTATT TATTTACTCAGTTGGCAAGTCTCC and the primer pair GGAAAAC ACTTGGCAAAGAAGAAAAAACAGAATAATGTATCC and TAGCGAAAA ATCCTTTTCTTTCTTACCCTTCTCCATCAGTGTTCAATAAATCATC, respectively. The three fragments were cloned into the pSG-thrC-Phspank backbone (Supplementary File 1) using the NEBuilder HiFI DNA Assembly cloning kit (NEB, no. E5520S) and transformed to

DH5α-competent cells. The cloned vector was subsequently transformed into the thrC site of *B. subtilis* BEST7003.

The *tad1*-containing *B. subtilis* BEST7003 strain was then infected with phage SBSphiJ with an MOI of 0.1 and cell lysate was collected. The lysate was used to infect a Thoeris-containing *B. subtilis* culture in two consecutive rounds with an MOI of 2. Several plaques were collected and screened using PCR for *tad1*-containing phages. A *tad1*-contaning phage was purified three times on *B. subtilis* BEST7003. Purified phage was verified again for the presence of *tad1* using PCR amplification. Whole-genome sequencing was then applied to the phage, and Breseq analysis[33] was used to verify the integrity of the *tad1* knock-in.

Identification of anti-Thoeris homologues and phylogenetic reconstruction

Tad1 homologues were searched for in the database MGV[11] and in approximately 38,000 prokaryotic genomes that were downloaded from the IMG database[10] in October 2017. The search was preformed using the 'search' option of MMseqs release 12-113e3, with default parameters. Unique (non-redundant) sequences were used for multiple alignment with MAFFT v.7.402 (ref. [35]) using default parameters. The phylogenetic tree was constructed using IQ-TREE v.1.6.5 (ref. [36]) with the '-m LG' parameter. The online tool iTOL24 (v.5)[37] was used for tree visualization. Phage family annotations were based on prediction in the MGV database. Host phylum annotations were based either on prediction in the MGV database or the IMG taxonomy of the bacteria in which the prophage was found.

Preparation of filtered cell lysates

For in vivo experiments we used *B. subtilis* BEST7003 co-expressing a Thoeris system in which ThsA was mutated in its NADase active site ($ThsA_{N112A}$ + ThsB)[1] under its native promoter, and Tad1 under the Physpank promoter. Controls included cells expressing only the mutated Thoeris system, as well as those lacking both the Thoeris system and Tad1. These cultures were grown overnight and then diluted 1:100 in 350 ml of MMB supplemented with 1 mM IPTG and grown at 37 °C, with shaking at 200 rpm for 90 min. Each culture was then incubated and shaken at 25 °C, 200 rpm until reaching an OD_{600} of 0.3. At this point, a sample of 50 ml was taken as the uninfected (time 0 min) sample and phage SBSphiJ or SBSphiJ7 was added to the remaining 300 ml of culture at an MOI of 5. Flasks were incubated at 25 °C with shaking (200 rpm) for the duration of the experiment. Samples (50 ml) were collected at time points 75, 90, 105 and 120 min post infection. Immediately following sample removal (including time point 0 min), the 50 ml sample tubes were placed on ice and centrifuged at 4 °C for 10 min to pellet the cells. The supernatant was discarded and the pellet flash-frozen and stored at −80 °C.

For the in vitro experiment with purified cmTad1, *B. subtilis* BEST7003 cultures overexpressing the Thoeris ThsB protein under the Physpank promoter, together with control cultures, were diluted 1:100 in 200 ml of MMB supplemented with 0.1 mM IPTG and grown at 37 °C, with shaking at 200 rpm. After 90 min the temperature was lowered to 25 °C and samples were shaken (200 rpm) until reaching an OD_{600} of 0.3. The SBSphiJ phage was then added to the culture at an MOI of 5. Flasks were incubated at 25 °C with shaking (200 rpm). At 120 min post infection the culture was collected into 50 ml tubes, centrifuged for 10 min at 4 °C, supernatant discarded and the pellet stored at −80 °C.

To extract cell metabolites from frozen pellets, 600 µl of 100 mM Na phosphate buffer (pH 8.0) supplemented with 4 mg ml^{-1} lysozyme (Sigma, no. L6876) was added to each pellet. Tubes were then incubated for 10 min at 25 °C and returned to ice. Samples were transferred to FastPrep Lysing Matrix B in a 2 ml tube (MP Biomedicals, no. 116911100) and lysed at 4 °C using a FastPrep bead beater for 2 × 40 s at 6 m s^{-1}. Tubes were then centrifuged at 4 °C for 10 min at 15,000*g*. Supernatant was then transferred to an Amicon Ultra-0.5 Centrifugal Filter Unit 3 kDa (Merck Millipore, no. UFC500396) and centrifuged for 45 min at 4 °C, 12,000 *g*. Filtered lysates were taken for either LC–MS analysis or in vitro NADase activity assay.

LC–MC monitoring of the Thoeris cADPR isomer

Sample analysis was carried out by MS-Omics as follows. Samples were diluted 1:3 in 10% ultra-pure water and 90% acetonitrile containing 10 mM ammonium acetate at pH 9.0, then filtered through a Costar Spin-X centrifuge tube filter with a 0.22 µm nylon membrane. The analysis was carried out using an ultra-performance LC (UPLC) system (Vanquish, Thermo Fisher Scientific) coupled with a high-resolution, quadrupole-orbitrap mass spectrometer (Q Exactive HF Hybrid Quadrupole-Orbitrap, Thermo Fisher Scientific). The standard cADPR peak was identified using a synthetic standard (cADPR: Sigma-Aldrich, no. C7344) run. UPLC was performed using an InfinityLab PoroShell 120 hydrophilic interaction chromatography (HILIC-Z PEEK) lined column with dimensions of 2.1 × 150 mm^2 and a particle size of 2.7 µm (Agilent Technologies). The composition of mobile phase A was 10 mM ammonium acetate at pH 9.0 in 90% acetonitrile LC–MC grade (VWR Chemicals) and 10% ultra-pure water from a Direct-Q 3 UV Water Purification System with LC-Pak Polisher (Merck KGaA); mobile phase B was 10 mM ammonium acetate at pH 9.0 in ultra-pure water with 15 µM medronic acid (InfinityLab Deactivator additive, Agilent Technologies). The flow rate was kept at 250 µl ml^{-1}, consisting of a 2 min hold at 10% B, increased to 40% B at 14 min, held till 15 min, decreased to 10% B at 16 min and held for a further 8 min. The column temperature was set at 30 °C and an injection volume of 5 µl. Analysis was performed in positive ionization mode at m/z = 200–1,000 and a mass resolution of 120,000 (m/z = 200). An electrospray ionization interface was used as the ionization source. Peak areas were extracted using TraceFinder 4.1 (Thermo Fisher Scientific) with an accepted deviation of 5 ppm. Fragmentation was done through a higher-energy collisional dissociation cell using normalized collision energy of 20, 40 and 60 eV, where the spectrum is the sum of each collision energy.

CmTad1 protein cloning, expression and purification for experiments with cell lysates

Cl. mangenotii Tad1 (cmTad1) was used for in vitro experiments because its higher stability enabled long-term storage at −80 °C. The *cmTad1* gene was cloned into the expression vector pET28-bdSumo using the restriction-free method[38] (Supplementary File 3). pET28-bdSumo was constructed by transfer of the His14-bdSUMO cassette from the K151 expression vector, generously provided by D. Görlich from the Max-Planck-Institute, Göttingen[39], into the expression vector pET28-TevH[40].

CmTad1 was expressed in *E. coli* BL21(DE3) by induction with 200 µM IPTG at 15 °C overnight. The culture was harvested and lysed by a cooled cell disrupter (Constant Systems) in a lysis buffer (50 mM Tris pH 8.0, 0.5 M NaCl, 1 mM DTT, 2 mM $MgCl_2$ and 250 mM sucrose) containing 200 KU 100 ml^{-1} lysozyme, 20 µg ml^{-1} DNase, 1 mM phenylmethylsulfonyl fluoride and protease inhibitor cocktail (Millipore, no. 539134). After centrifugation, the supernatant of the lysate was incubated with 5 ml of Nickel-beads (Adar Biotech; prewashed with lysis buffer) for 1 h at 4 °C. After removal of the supernatant by centrifugation, the beads were washed three times with 50 ml of lysis buffer and once with lysis buffer containing 50 mM imidazole (1 mM tris(2-carboxyethyl)phosphine (TCEP) replacing DTT). CmTad1 was eluted from the beads by incubation with 20 ml of cleavage buffer (50 mM Tris pH 8.0, 0.5 M NaCl, 1 mM DTT, 2 mM $MgCl_2$, 250 mM sucrose and 0.4 mg bdSumo protease) for 2 h at 25 °C. The supernatant containing the cleaved cmTad1 was removed and an additional 20 ml of cleavage buffer was added to the beads and left overnight at 4 °C. The two elution samples were combined, concentrated and applied to a size-exclusion column (HiLoad 16/60 Superdex200 prep-grade, Cytiva) equilibrated with a SEC buffer (50 mM Tris pH 8.0, 50 mM NaCl and 1 mM DTT). Fractions containing pure cmTad1 were pooled and frozen at −80 °C.

NADase activity assay as a reporter for the cADPR isomer

NADase assay was performed by using the *B. cereus* MSX-D12 ThsA enzyme as a reporter for the presence of the cyclic ADPR isomer[1]. The reporter enzyme ThsA was expressed and purified as described previously[1]. NADase reaction was performed in black, 96-well, half-area plates (Corning, no. 3694) at 25 °C in a 50 µl final reaction volume. Next, 5 µl of 5 mM εNAD (Sigma, no. N2630) solution was added to each well sample immediately before measurement and mixed by pipetting. εNAD was used as a fluorogenic substrate to report ThsA enzyme NADase activity by monitoring increase in fluorescence (excitation 300 nm, emission 410 nm) using a Tecan Infinite M200 plate reader at 25 °C. Reaction rate was derived from the linear part of the initial reaction.

For assessment of the in vivo activity of Tad1 in cells co-expressing both ThsB (native promoter) and Tad1, filtered lysates were mixed directly with ThsA followed by the addition of εNAD. Controls included filtered lysates derived from cells expressing ThsB (without Tad1), and from cells expressing neither ThsB nor Tad1. For assessment of the in vitro activity of purified cmTad1, phage-infected, cell-filtered lysate (diluted 1:16–1:20) overexpressing ThsB (100 µM IPTG) was incubated with purified cmTad1 (150–600 nM final concertation) at 25 °C. Controls included filtered lysates incubated with diluted SEC buffer.

To examine the level of the cADPR isomer after cmTad1 heat inactivation, cmTad1 (600nM) was incubated with phage-infected, cell-filtered lysate (diluted 1:16) for 10 min at 25 °C followed by incubation at either 85 or 25 °C for an additional 5 min. Samples were then mixed with 2 µl of 2.5 µM ThsA and 5 µl of 5 mM εNAD and fluorescence was monitored as described above.

Protein expression and purification for biochemistry and crystallization analyses

CmTad1, cbTad1, cmTad1 mutants and $AaTIR^{TIR}$ (AaTIR Δ145–327) genes were cloned from synthetic DNA fragments (Integrated DNA Technologies) by Gibson assembly into a custom pET expression vector containing an N-terminal 6× His-SUMO2 tag and an ampicillin resistance gene, as previously described[41]. Plasmids were transformed into BL21(DE3) RIL *E. coli* (Agilent) and colonies grown on MDG agar plates (1.5% agar, 2 mM $MgSO_4$, 0.5% glucose, 25 mM Na_2HPO_4, 25 mM KH_2PO_4, 50 mM NH_4Cl, 5 mM Na_2SO_4, 0.25% aspartic acid and 2–50 µM trace metals). Three colonies were picked into a 30 ml MDG starter culture and grown overnight at 37 °C with 230 rpm shaking. Then, 15 ml of overnight cultures was used to seed 1 l of M9ZB expression culture (2 mM $MgSO_4$, 0.5% glycerol, 47.8 mM Na_2HPO_4, 22 mM KH_2PO_4, 18.7 mM NH_4Cl, 85.6 mM NaCl, 1% Cas-amino acids, 2–50 µM trace metals, 100 µg ml^{-1} ampicillin and 34 µg ml^{-1} chloramphenicol). Expression cultures were grown at 37 °C with 230 rpm shaking to an OD_{600} of 2.0–2.5 before induction of expression with 0.5 mM IPTG and incubation of cultures at 16 °C with 230 rpm shaking for 16–20 h. Selenomethionine-labelled protein was produced as previously described, by growing expression cultures in modified M9ZB medium (2 mM $MgSO_4$, 0.4% glucose, 47.8 mM Na_2HPO_4, 22 mM KH_2PO_4, 18.7 mM NH_4Cl, 85.6 mM NaCl, 2–50 µM trace metals, 1 µg ml^{-1} thiamine, 100 µg ml^{-1} ampicillin and 34 µg ml^{-1} chloramphenicol)[42]. After expression, 2 l of culture was harvested by centrifugation and resuspended in 120 ml of lysis buffer (20 mM HEPES-KOH pH 7.5, 400 mM NaCl, 30 mM imidazole, 10% glycerol and 1 mM DTT). Cells were lysed by sonication then clarified by centrifugation at 25,000 *g* for 20 min, and lysate was passed over 8 ml of Ni-NTA resin (Qiagen) using gravity chromatography. Resin was washed with 70 ml of wash buffer (20 mM HEPES-KOH pH 7.5, 1 M NaCl, 30 mM imidazole, 10% glycerol and 1 mM DTT) and 20 ml of lysis buffer, then eluted with lysis buffer containing 300 mM imidazole. Eluate was dialysed overnight using 14 kDa dialysis tubing in dialysis buffer (20 mM HEPES-KOH pH 7.5, 250 mM KCl and 1 mM TCEP) in the presence of recombinant human-SENP2 to induce SUMO-tag cleavage. For crystallography, proteins were purified further by size-exclusion chromatography using a Superdex 75 16/600 column (Cytiva). Size-exclusion peaks of interest (crystallography) or dialysed Ni-NTA elutions (biochemistry) were collected and concentrated to over 40 mg ml^{-1}, then flash-frozen and stored at −80 °C.

ThsB′, a second TIR domain containing the ThsB gene (IMG ID 2519697834) that is part of the double-TIR Thoeris defence system naturally occurring in *B. cereus* MSX-D12, and that produces the signalling molecule in vitro in the presence of NAD^+, was cloned as described above into a custom pET expression vector containing a C-terminal 6× His tag and a chloramphenicol resistance gene. Expression and purification were carried out as described above, except that plasmids were transformed into BL21 (DE3) cells, cultures were grown in the presence of chloramphenicol only and protein was concentrated to around 4 mg ml^{-1}, flash-frozen and stored immediately after dialysis.

Ligand-bound Tad1 was produced by first co-expressing cmTad1 with BdTIR. BdTIR was cloned into a custom pET vector containing a C-terminal Twin-Strep tag, a chloramphenicol resistance gene and an IPTG-inducible promoter (BdTIR-strep). Plasmids containing cmTad1 or cbTAD1 were co-transformed with BdTIR-strep into BL21(DE3) cells then plated onto MDG agar plates and expressed as described above. Ligand-bound Tad1 was purified as described above, with a modified method. After elution from Ni-NTA resin using 300 mM imidazole, eluate was treated with recombinant human-SENP2 for 1 h to induce SUMO-tag cleavage then immediately purified further by size-exclusion chromatography. Peaks of interest were collected and concentrated to over 25 mg ml^{-1}, then flash-frozen and stored at −80 °C.

Tad1 crystallization and structural analysis

Crystals of cbTad1 were grown using the hanging-drop method in EasyXtal 15-well trays (NeXtal). Samples were prepared by first diluting purified protein to 10 mg ml^{-1} using buffer containing 20 mM HEPES-KOH pH 7.5, 80 mM KCl and 1 mM TCEP. Two microlitres of hanging drops were set at a 1:1 ratio of protein to reservoir solution over a well with 400 µl of reservoir solution. Each protein was crystallized using the following conditions: (1) native or selenomethionine-labelled cbTad1 in the apo state: crystals were grown for 1–2 weeks using reservoir solution containing 0.1 M Tris-HCl pH 7.5 and 40% PEG 200 before being harvested by flash-freezing in liquid nitrogen. (2) cbTad1 complexed with 1′′–2′ gcADPR: using cbTad1 purified from cells expressing BdTIR, crystals were grown for 1–5 days using reservoir solution containing 0.1 M 2-(*N*-morpholino)ethanesulfonic acid pH 5.0, 1% PEG-6000 and 300 µM 1′′–2′ gcADPR before being cryoprotected with reservoir solution containing 35% ethylene glycol and harvested by flash-freezing in liquid nitrogen. X-ray diffraction data were collected at the Advanced Photon Source (beamlines 24-ID-C and 24-ID-E), and data were processed using the SSRL autoxds script (A. Gonzalez, Stanford SSRL). Anomalous data for phase determination were collecting using selenomethionine-labelled crystals. Heavy sites were identified and initial maps produced using AutoSol in Phenix[43]. Model building was performed in Coot[44], with refinement in Phenix, and statistics were analysed as presented in Extended Data Table 1 (refs. [45–47]). Final structures were refined to stereochemistry statistics for Ramachandran plot (favoured/allowed), rotamer outliers and MolProbity score as follows: cbTad1 SeMet apo, 98.60/1.40%, 0.20%, 1.11; cbTad1–1′′–2′-gcADPR, 99.19/0%, 0%, 1.00. See Extended Data Table 1 and Data Availability for deposited PDB codes. All structure figures were generated with PyMOL 2.3.0.

cmTad1 ligand-binding site residue substitution and in vivo analysis

Amino acid substitutions of the *cmTad1* gene were generated using the plasmid pSG-thrC-Phspank-cmTad1 (Supplementary File 4) as a PCR template, followed by ligation using KLD Enzyme Mix (NEB, no. M0554). All primers used for amino acid substitution are listed in Supplementary Table 5. The ligated products were then transformed into NEB 5-alpha-competent *E. coli* (NEB, no. C2987). Plasmids containing amino acid substitution in *cmTad1* were then transformed into *B. subtilis* BEST7003 cells containing

the Thoeris defence system, resulting in cultures co-expressing both Thoeris and mutated cmTad1. Efficiency of plating was used, as described above, to compare plaque assay results between bacteria containing the defence system with WT or amino acid-substituted *cmTad1* gene.

Purification of 1′′–2′ gcADPR

To isolate 1′′–2′ gcADPR, purified and concentrated (over 1 mM) cmTad1 co-expressed with BdTIR in storage buffer (20 mM HEPES-KOH pH 7.5, 250 mM KCl and 1 mM TCEP) was denatured by boiling at 95 °C for 5 min. Denatured cmTad1 was pelleted at 13,500 *g* for 10 min and supernatant was passed through a 0.5 ml 10 kDa filter (Amicon). 1′′–2′ gcADPR concentration was estimated using the extinction coefficient of cADPR and absorbance at 260 nm.

In vitro cmTad1 mutant analysis of 1′′–2′ gcADPR binding

Individual cmTad1 mutants (125 µM of each) were incubated with 25 µM 1′′–2′ gcADPR in ThsA buffer (20 mM HEPES-KOH pH 7.5 and 80 mM KCl) at room temperature for 10 min before being passed through a 10 kDa filter. Filtrates were analysed by ThsA NADase activity assay in comparison with buffer and 25 µM 1′′–2′ gcADPR controls.

NMR

For NMR analysis, 1′′–2′ gcADPR-bound cmTad1 was purified as detailed above except that all buffers containing HEPES-KOH used during the purification process were replaced with similar buffers containing equimolar amounts of phosphate buffer (16 mM Na_2HPO_4 and 4 mM KH_2PO_4, pH 7.5) and lacking reducing agents. 1′′–2′ gcADPR-bound cmTad1 in modified storage buffer (16 mM Na_2HPO_4, 4 mM KH_2PO_4 pH 7.5 and 250 mM KCl) was washed extensively by repeated dilution with water using a 10 kDa concentration unit, before denaturation by boiling at 95 °C for 15 min. Denatured cmTad1 was pelleted at 13,500 *g* for 20 min and supernatant was passed through a 0.5 ml 10 kDa filter (Amicon). Supernatant containing 1′′–2′ gcADPR was dried using a Vacufuge concentrator (Eppendorf) and resuspended in D_2O to a final yield of about 0.5 ml of 5 mM 1′′–2′ gcADPR (approximately 1.4 mg) in a 5 mm NMR tube rated for 600 MHz.

A Bruker Avance II 600 MHz Bio-molecular NMR System with a Prodigy cryoprobe was used to acquire 1d ^{1}H, 1d ^{13}C, ^{1}H-^{1}H gCOSY, ^{1}H-^{1}H ROESY, ^{1}H-^{13}C HMBC, ^{1}H-^{13}C HSQC and ^{1}H-^{15}N HMBC spectra at 298K. NMR data were processed and analysed with MestreNova software. The chemical shift assignments of ribose atoms were primarily obtained from gCOSY and ROESY datasets. The unique ribose–ribose cyclization bond of 1′′–2′ gcADPR was validated by a pair of three-bond J-coupling peaks between the cyclized ribose 1′′ atoms and adenosine ribose 2′ atoms in the ^{13}C-HMBC spectrum. The connectivity between adenine and adenosine ribose was established through the three-bond ^{13}C-HMBC peak between ^{13}C resonance of carbon 8 and ^{1}H resonance of proton 1′, as well as by the three-bond ^{15}N-HMBC peak between ^{15}N resonance of nitrogen 9 and ^{1}H resonance of proton 2′.

HPLC

Individual samples were injected (15–75 µl) onto a C18 column (Zorbax Bonus-RP 4.6 × 150 mm^2, 3.5 µm) attached to an Agilent 1200 Infinity Series LC system and eluted isocratically at 40 °C at a flow rate of 1 ml min^{-1} with 50 mM Na_2HPO_4 pH 6.8 supplemented with 3% acetonitrile. Buffer was adjusted to pH 5.2 for samples relating to 1′′–2′ gcADPR, due to overlap of the NAD^+ peak at pH 6.8. Elution profiles were monitored at an absorbance of 254 nm. To obtain pure 1′′–3′ gcADPR, the peak from 2.9 to 3.4 min was collected as one fraction from cmTad1-enriched 1′′–3′ gcADPR.

BdTIR filtrate preparation

BdTIR-strep was cloned into BL21(DE3) cells then plated onto MDG agar plates and expressed as described above. Cells from 50 ml of expression culture were pelleted at 3,200*g* for 10 min and resuspended in 1 ml of ThsA reaction buffer (20 mM HEPES-KOH pH 7.5 and 80 mM KCl) before lysis by sonication and clarification by centrifugation at 13,500*g* for 10 min. Supernatant was then boiled at 95 °C for 15 min, denatured proteins were pelleted at 13,500*g* for 20 min and supernatant was passed through a 0.5 ml 10 kDa filter (Amicon).

Filtrate was then treated for 5 min with storage buffer, 1 mM cmTad1 or 1 mM cmTad1 and subsequent boiling before passage through a 10 kDa filter, and analysed by HPLC or diluted 1:20 in ThsA reaction buffer and analysed by ThsA NADase activity assay.

Purification of ThsB cADPR isomer from ThsB′

Purified ThsB′ was used to set up 50 ml reactions (50 mM sodium phosphate pH 8.0, 8 mM HEPES-KOH pH 7.5, 100 mM KCl, 1 mM NAD^+ and 16 µM ThsB′). Reactions were carried out at room temperature for 1.5 h before boiling at 95 °C for 15 min, pelleting at 13,500 *g* for 20 min and filtering through a 0.5 ml 10 kDa filter (Amicon). An aliquot of filtrate was taken for analysis by HPLC or diluted 1:20 in ThsA reaction buffer and analysed by ThsA NADase activity assay.

To purify the ThsB′ cADPR isomer, filtrate was chilled on ice for 10 min before the addition of 100 µM cmTad1 for 10 min. The mixture was then concentrated to 1 ml, diluted with storage buffer (20 mM HEPES-KOH pH 7.5 and 250 mM KCl) and concentrated again to 1 ml in a 10 kDa concentration unit before boiling at 95 °C for 15 min, pelleting at 13,500*g* for 20 min and filtering through a 0.5 ml 10 kDa filter (Amicon). The cADPR isomer was further purified by HPLC fractionation of the enriched peak (2.9–3.4 min).

Production of 1′′–3′ gcADPR from AaTIR^{TIR}

Purified AaTIR^{TIR} was used to set up 150 µl reactions (56 mM Tris-HCl pH 7.5, 10 mM KCl, 5 mM DTT, 20 mM NAD^+ and 3.3 µM AaTIR^{TIR}) based on previously described methods[14]. Reactions were carried out at room temperature for 1 h before being filtered through a 10 kDa filter. Filtrate was then treated for 5 min with storage buffer, 5 mM cmTad1 or 5mM cmTad1 and subsequent boiling before being passed through a 10 kDa filter, and analysed by HPLC or diluted 1:1,000 in ThsA reaction buffer and analysed by ThsA NADase activity assay. 1′′–3′ gcADPR was further purified by HPLC fractionation.

Isothermal titration calorimetry of 1′′–2′ gcADPR and cmTad1

Isothermal titration calorimetry (ITC) measurements were performed on a MicroCal Auto-iTC200 instrument (GE Healthcare). cmTad1 was used in the cell at 23 µM, and 1′′–2′ gcADPR was used in the syringe at 238 µM. cmTad1 was dialysed overnight in degassed ITC buffer (20 mM HEPES-KOH pH 7.5, 250 mM KCl and 0.3% glycerol), and 1′′–2′ gcADPR was diluted into matched buffer. Data fitting and analysis were performed using Origin 7.

Reporting summary

Further information on research design is available in the Nature Research Reporting Summary linked to this article.

Data availability

Data that support the findings of this study are available within the article and its Supplementary Tables and Supplementary files. IMG/MGV accessions, protein sequences and nucleotide sequences appear in Supplementary Tables 2–4. Coordinates and structure factors of cbTad1 apo and cbTad1–1''–2' gcADPR have been deposited in the PDB under accession codes 7UAV and 7UAW. The genome sequences of phages SBSphiJ1–SBSphiJ7 have been deposited with GenBank under accession codes OM982668–OM982674, respectively. Source data are available for all the main figures and for Extended Data Figs. 3, 4, 6 and 7.

26. Kropinski, A. M., Mazzocco, A., Waddell, T. E., Lingohr, E. & Johnson, R. P. In *Bacteriophages: Methods and Protocols* (eds Clokie, M. R. J. & Kropinski, A. M.) 69–76 (Humana, 2009).

27. Baym, M. et al. Inexpensive multiplexed library preparation for megabase-sized genomes. *PLoS ONE* **10**, e0128036 (2015).
28. Martin, M. Cutadapt removes adapter sequences from high-throughput sequencing reads. *EMBnet J.* **17**, 10 (2011).
29. Nurk, S. et al. Assembling genomes and mini-metagenomes from highly chimeric reads. *Res. Comput. Mol. Biol.* **7821**, 158–170 (2013).
30. Hyatt, D. et al. Prodigal: prokaryotic gene recognition and translation initiation site identification. *BMC Bioinformatics* **11**, 119 (2010).
31. Mazzocco, A., Waddell, T. E. & Lingohr, R. P. J. In *Bacteriophages: Methods and Protocols* (eds Clokie, M. R. J. & Kropinski, A. M.) 81–85 (Humana, 2009).
32. Steinegger, M. & Söding, J. MMseqs2 enables sensitive protein sequence searching for the analysis of massive data sets. *Nat. Biotechnol.* **35**, 1026–1028 (2017).
33. Deatherage, D. E. & Barrick, J. E. In *Engineering and Analyzing Multicellular Systems* (eds Sun, L. & Shou, W.) 165–188 (Humana, 2014).
34. Garb, J. et al. Multiple phage resistance systems inhibit infection via SIR2-dependent NAD^+ depletion. *Nat. Microbiol*. https://doi.org/10.1038/s41564-022-01207-8 (2022).
35. Katoh, K. & Standley, D. M. MAFFT multiple sequence alignment software version 7: improvements in performance and usability. *Mol. Biol. Evol.* **30**, 772–780 (2013).
36. Nguyen, L.-T., Schmidt, H. A., von Haeseler, A. & Minh, B. Q. IQ-TREE: a fast and effective stochastic algorithm for estimating maximum-likelihood phylogenies. *Mol. Biol. Evol.* **32**, 268–274 (2015).
37. Letunic, I. & Bork, P. Interactive Tree Of Life (iTOL) v5: an online tool for phylogenetic tree display and annotation. *Nucleic Acids Res.* **49**, W293–W296 (2021).
38. Unger, T., Jacobovitch, Y., Dantes, A., Bernheim, R. & Peleg, Y. Applications of the Restriction Free (RF) cloning procedure for molecular manipulations and protein expression. *J. Struct. Biol.* **172**, 34–44 (2010).
39. Frey, S. & Görlich, D. A new set of highly efficient, tag-cleaving proteases for purifying recombinant proteins. *J. Chromatogr. A* **1337**, 95–105 (2014).
40. Peleg, Y. & Unger, T. In *Structural Proteomics* (eds Kobe, B., Guss, M. & Huber, T.) 197–208 (Humana, 2008).
41. Zhou, W. et al. Structure of the human cGAS-DNA complex reveals enhanced control of immune surveillance. *Cell* **174**, 300–311 (2018).
42. Eaglesham, J. B., Pan, Y., Kupper, T. S. & Kranzusch, P. J. Viral and metazoan poxins are cGAMP-specific nucleases that restrict cGAS-STING signalling. *Nature* **566**, 259–263 (2019).
43. Liebschner, D. et al. Macromolecular structure determination using X-rays, neutrons and electrons: recent developments in Phenix. *Acta Crystallogr. D Struct. Biol.* **75**, 861–877 (2019).
44. Emsley, P. & Cowtan, K. Coot: model-building tools for molecular graphics. *Acta Crystallogr. D Biol. Crystallogr.* **60**, 2126–2132 (2004).
45. Chen, V. B. et al. MolProbity: all-atom structure validation for macromolecular crystallography. *Acta Crystallogr. D Biol. Crystallogr.* **66**, 12–21 (2010).
46. Karplus, P. A. & Diederichs, K. Linking crystallographic model and data quality. *Science* **336**, 1030–1033 (2012).
47. Weiss, M. S. Global indicators of X-ray data quality. *J. Appl. Crystallogr.* **34**, 130–135 (2001).
48. Gilchrist, C. L. M. & Chooi, Y.-H. clinker & clustermap.js: automatic generation of gene cluster comparison figures. *Bioinformatics* **37**, 2473–2475 (2021).

Acknowledgements We thank the Sorek laboratory members for comments on the manuscript and fruitful discussion. We also thank Y. Peleg and S. Albeck from the Center for Structural Proteomics within the Weizmann Institute of Science for assistance with protein expression, M. Danielsen and D. Malheiro from MS-Omics for conducting MS experiments, S. C. Wilson for advice on gcADPR analysis and K. Arnett from Harvard University's Center for Macromolecular Interactions for assistance with the ITC experiments. R.S. was supported, in part, by the European Research Council (grant no. ERC-AdG GA 101018520), Israel Science Foundation (grant no. ISF 296/21), Deutsche Forschungsgemeinschaft (SPP 2330, grant no. 464312965), the Ernest and Bonnie Beutler Research Program of Excellence in Genomic Medicine, the Minerva Foundation with funding from the Federal German Ministry for Education and Research and the Knell Family Center for Microbiology. P.J.K. was supported, in part, by the Pew Biomedical Scholars programme and The Mathers Foundation. E.Y. is supported by the Israeli Council for Higher Education (CHE) via the Weizmann Data Science Research Center, B.R.M. is supported as a Ruth L. Kirschstein NRSA Postdoctoral Fellow (no. NIH F32GM133063) and S.J.H. is supported through a Cancer Research Institute Irvington Postdoctoral Fellowship (no. CRI3996). X-ray data were collected at Northeastern Collaborative Access Team beamlines 24-ID-C and 24-ID-E (no. P30 GM124165), including use of a Pilatus detector (no. S10RR029205), an Eiger detector (no. S10OD021527) and the Argonne National Laboratory Advanced Photon Source (no. DE-AC02-06CH11357).

Author contributions A. Leavitt isolated phages and conducted all in vivo experiments. E.Y. built and executed the computational pipeline and analysed data. G.A. performed biochemical experiments with cell lysates and led the mechanistic characterization of Tad1 activity. A. Lu performed the structural analysis of Tad1 and biochemically and structurally characterized TIR-derived signalling molecules. J.G. designed and helped with performing knock-in and knockdown experiments. E.H. helped with LC–MC data analysis. B.R.M. and S.J.H. helped with structural analysis and biochemical characterization of TIR-derived molecules. S.P.A. helped with ITC data collection and stoichiometry calculations. Z.-Y.J.S. performed NMR analysis. The study was supervised by P.J.K. and R.S. The manuscript was written by E.Y., A. Lu, P.J.K. and R.S. All authors contributed to editing the manuscript and support the conclusions.

Competing interests R.S. is a scientific cofounder and advisor of BiomX and Ecophage. The remaining authors declare no competing interests.

Additional information

Supplementary information The online version contains supplementary material available at https://doi.org/10.1038/s41586-022-05375-9.

Correspondence and requests for materials should be addressed to Philip J. Kranzusch or Rotem Sorek.

Peer review information *Nature* thanks Joseph Bondy-Denomy and the other, anonymous, reviewer(s) for their contribution to the peer review of this work. Peer reviewer reports are available.

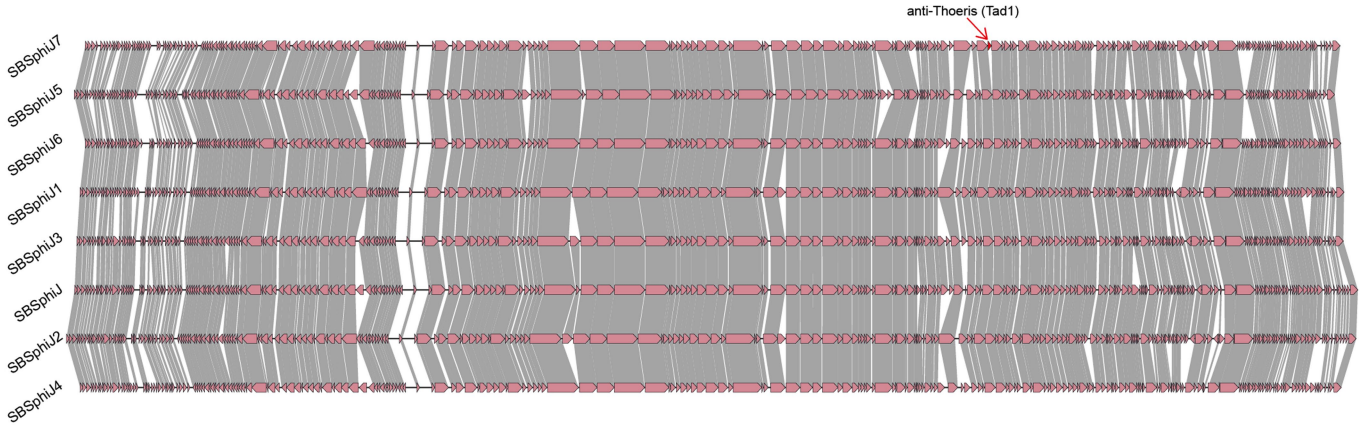

Extended Data Fig. 1 | Genome comparison of eight phages from the SBSphiJ group. Amino acid sequence similarity between the ORFs is marked by grey shading. Genome similarity was visualized using clinker[48].

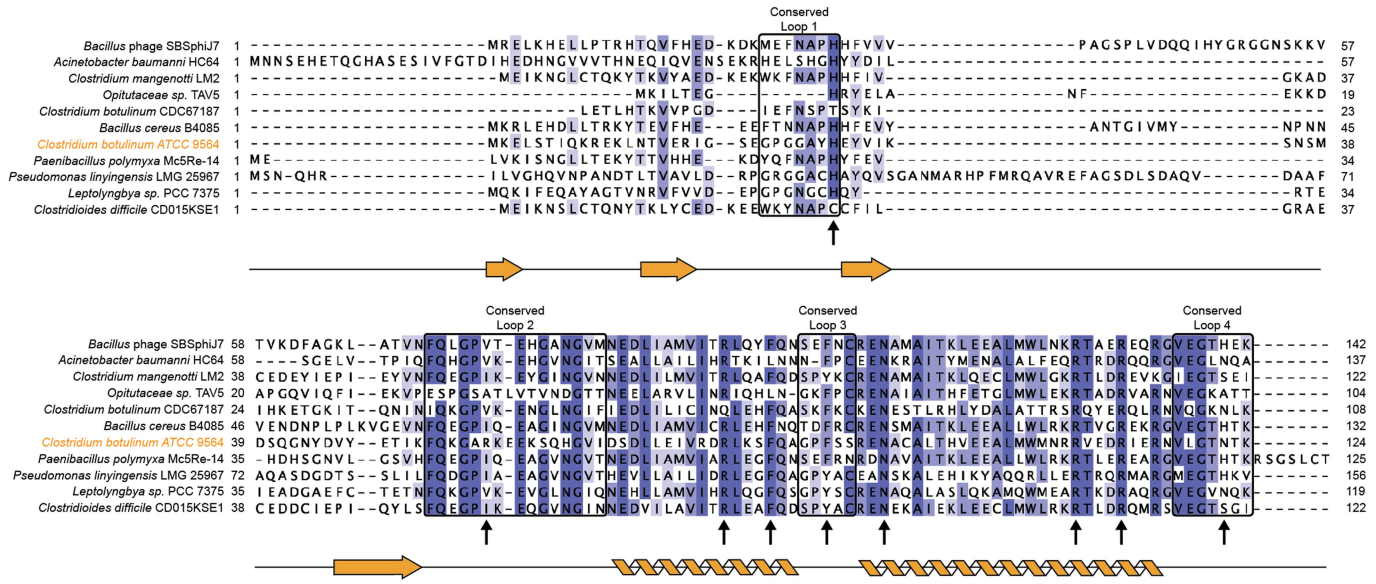

Extended Data Fig. 2 | Multiple sequence alignment of the original Tad1 from phage SBSphiJ7, and 10 Tad1 homologs that were verified experimentally as anti Thoeris proteins. The strength of shading indicates degree of residue conservation. The determined *Clostridium botulinum ATCC* 9564 (orange highlight) Tad1 secondary structure is depicted below, conserved loops involved in ligand-binding are boxed in black, and ligand-binding residues are marked with arrows.

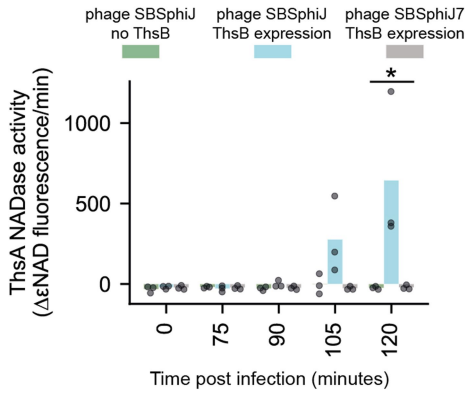

Extended Data Fig. 3 | Lysates derived from cells infected by phage SBSphiJ7 do not activate ThsA. Cells expressing ThsB (native promoter) were infected with phage SBSphiJ or phage SBSphiJ7 at multiplicity of infection (MOI) of 5. Control cells that do not express ThsB were infected with phage SBSphiJ. Shown is the activation of ThsA NADase activity by lysates from the infected cells. Purified ThsA used in this experiment is from a different batch than that used in Fig. 3, and hence the background activity of ThsA is different in the two assays. Bars represent the mean of three experiments, with individual data points overlaid. Asterisk marks a statistically significant difference in NADase activity (one-way ANOVA, $P = 0.039$).

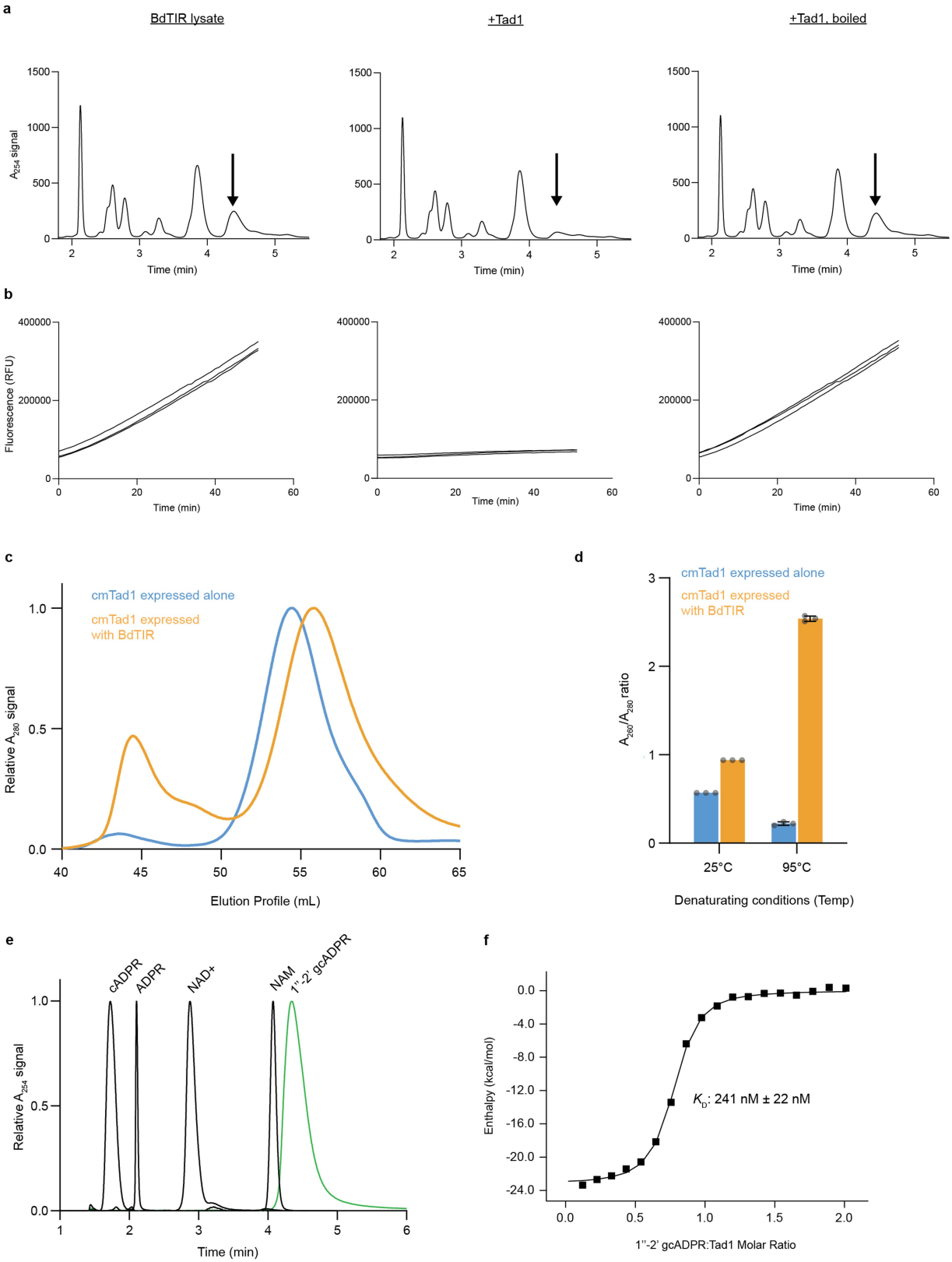

Extended Data Fig. 4 | See next page for caption.

Extended Data Fig. 4 | Purification and characterization of 1″–2′ gcADPR from BdTIR. a, HPLC analysis of filtered lysate from *E. coli* expressing a strep-tagged BdTIR after treatment with buffer, cmTad1, or cmTad1 and subsequent boiling. cmTad1 selectively binds, and upon boiling, releases 1″–2′ gcADPR. **b**, Filtered lysates from panel **a** were diluted 1:20 for stimulation of ThsA NADase activity. Data from three replicates are presented. **c**, Superdex 75 16/600 size-exclusion chromatography of 1″–2′ gcADPR-bound or *apo* state cmTad1 purified from cells expressing BdTIR or only cmTad1, respectively. 1″–2′ gcADPR-bound cmTad1 shows an ~0.8 mL right shift compared to cmTad1 in the *apo* state. **d**, A_{260}/A_{280} signal ratios of *apo* state and 1″–2′ gcADPR-bound cmTad1 in folding (25 °C) or denaturing (95 °C) conditions. 1″–2′ gcADPR-bound cmTad1 shows a higher A_{260}/A_{280} ratio and yields high A_{260} absorbance upon heat denaturation. Data are presented as mean values +/− SEM. **e**, HPLC analysis demonstrating that BdTIR-derived, cmTad1-purified 1″–2′ gcADPR migrates as a single, unique peak. 1″–2′ gcADPR separates from relevant molecule standards at pH = 5.1. **f**, Isothermal titration calorimetry measurement of cmTad1 affinity for 1″–2′ gcADPR. Data shown are representative of three individual experiments.

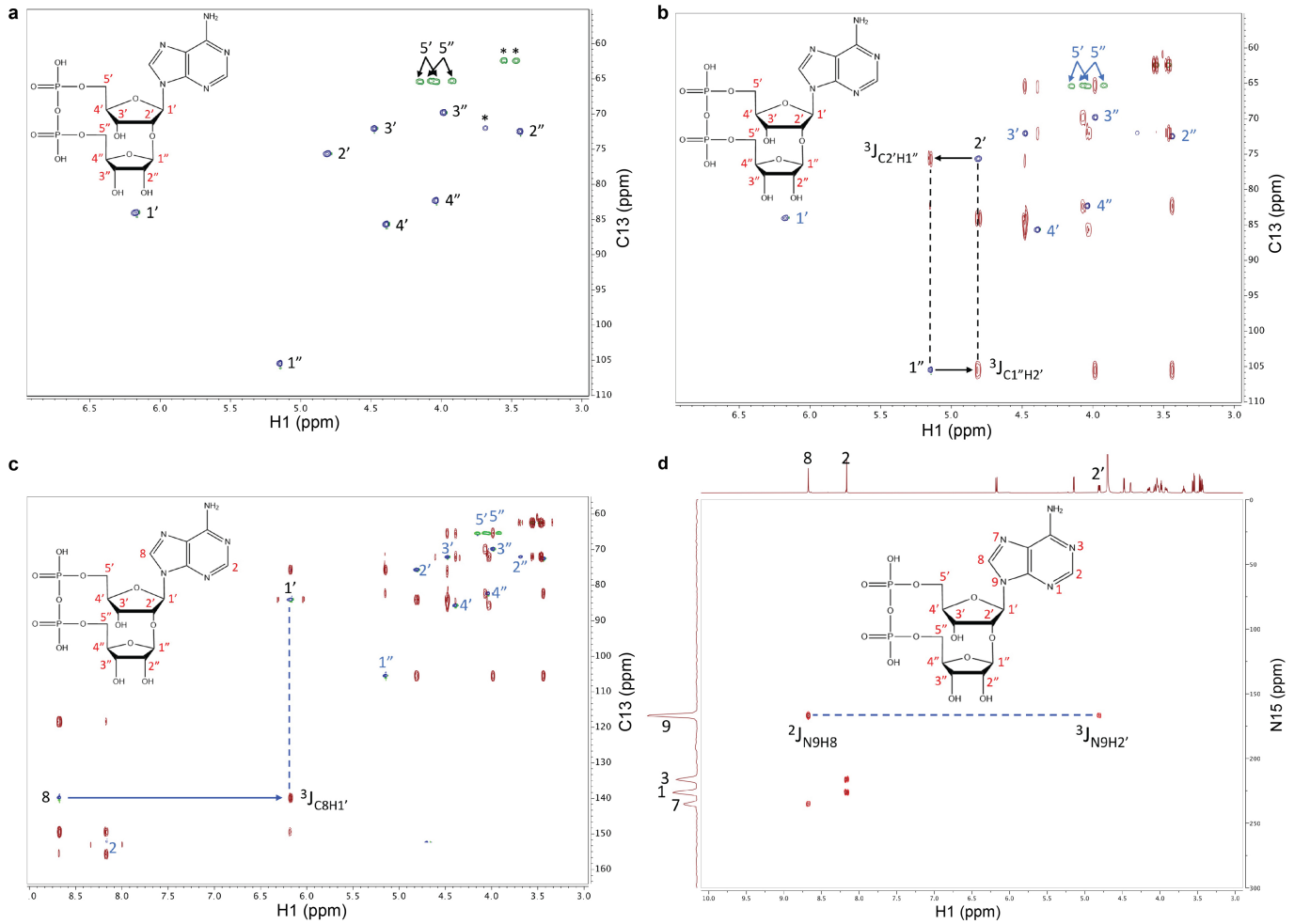

Extended Data Fig. 5 | NMR analysis of 1′′–2′ gcADPR from BdTIR. **a**, ^{13}C-HSQC spectrum of 1′′–2′ gcADPR showing assignments of the two ribose rings. Extraneous peaks from glycerol contaminants are marked with * symbols. **b**, ^{13}C-HMBC spectrum (red) superimposed on to the ^{13}C-HSQC spectrum (blue/green). The 3-bond J-coupled cross peaks between the 2′ and 1′′ positions of the two ribose rings are shown with black arrows. **c**, ^{13}C-HMBC spectrum (red) showing the 3-bond J-coupled peak (marked with a blue arrow) between ^{13}C resonance of carbon 8 and the ^{1}H resonance of the 1' proton. **d**, ^{15}N-HMBC spectrum showing the 3-bond J-coupled peak between ^{15}N resonance of nitrogen 9 and ^{1}H resonance of 2′ proton, aligned with the 2-bond J-coupled peak between ^{15}N resonance of nitrogen 9 and ^{1}H resonance of proton 8.

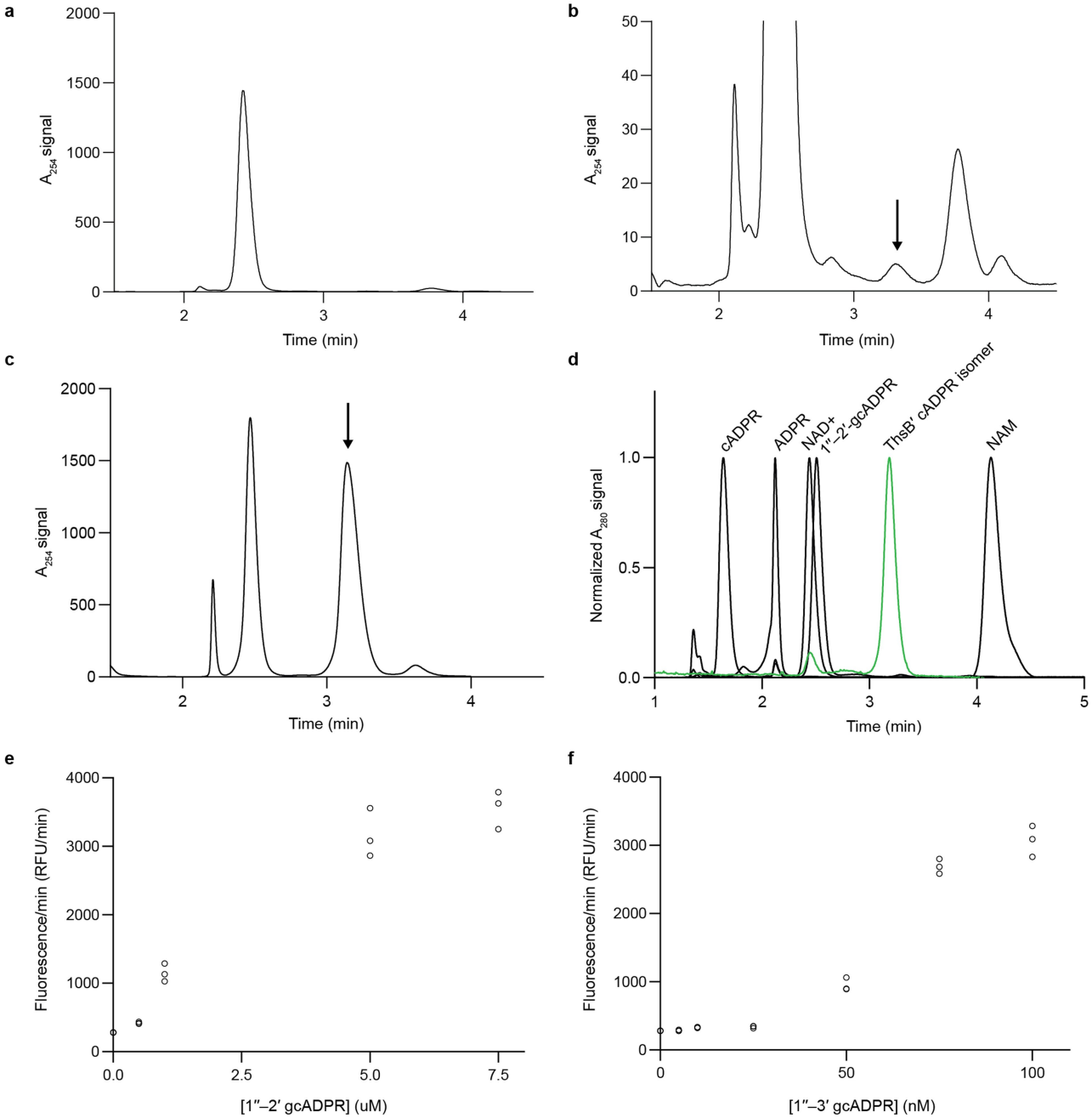

Extended Data Fig. 6 | Purification of the cADPR isomer from ThsB′ TIR domain and comparison to 1′′–2′ gcADPR. a, Purified ThsB′ (methods) was incubated with NAD^+ and the reaction products were filtered and analyzed by HPLC. **b**, Y-axis zoom of (a). The predicted ThsA-activating ThsB′ reaction product (ThsB′ cADPR isomer) is indicated with an arrow. **c**, HPLC analysis of the ThsB′ cADPR isomer reaction after addition of cmTad1 followed by concentration and heat denaturation demonstrates that cmTad1 is able to purify and enrich the predicted ThsB′ cADPR isomer peak. This peak was further isolated by HPLC fractionation. **d**, HPLC analysis shows that the cmTad1-purified ThsB′ cADPR isomer migrates as a unique peak with a small amount of residual NAD^+. ThsB′ cADPR isomer is distinct from 1′′–2′ gcADPR and separates from relevant molecule standards at pH = 6.8. (**e**-**f**) ThsA NADase activation curves of 1′′–2′ gcADPR (**e**) and 1′′–3′ gcADPR (**f**). ThsA activation is ~50–100× more sensitive to 1′′–3′ gcADPR than 1′′–2′ gcADPR.

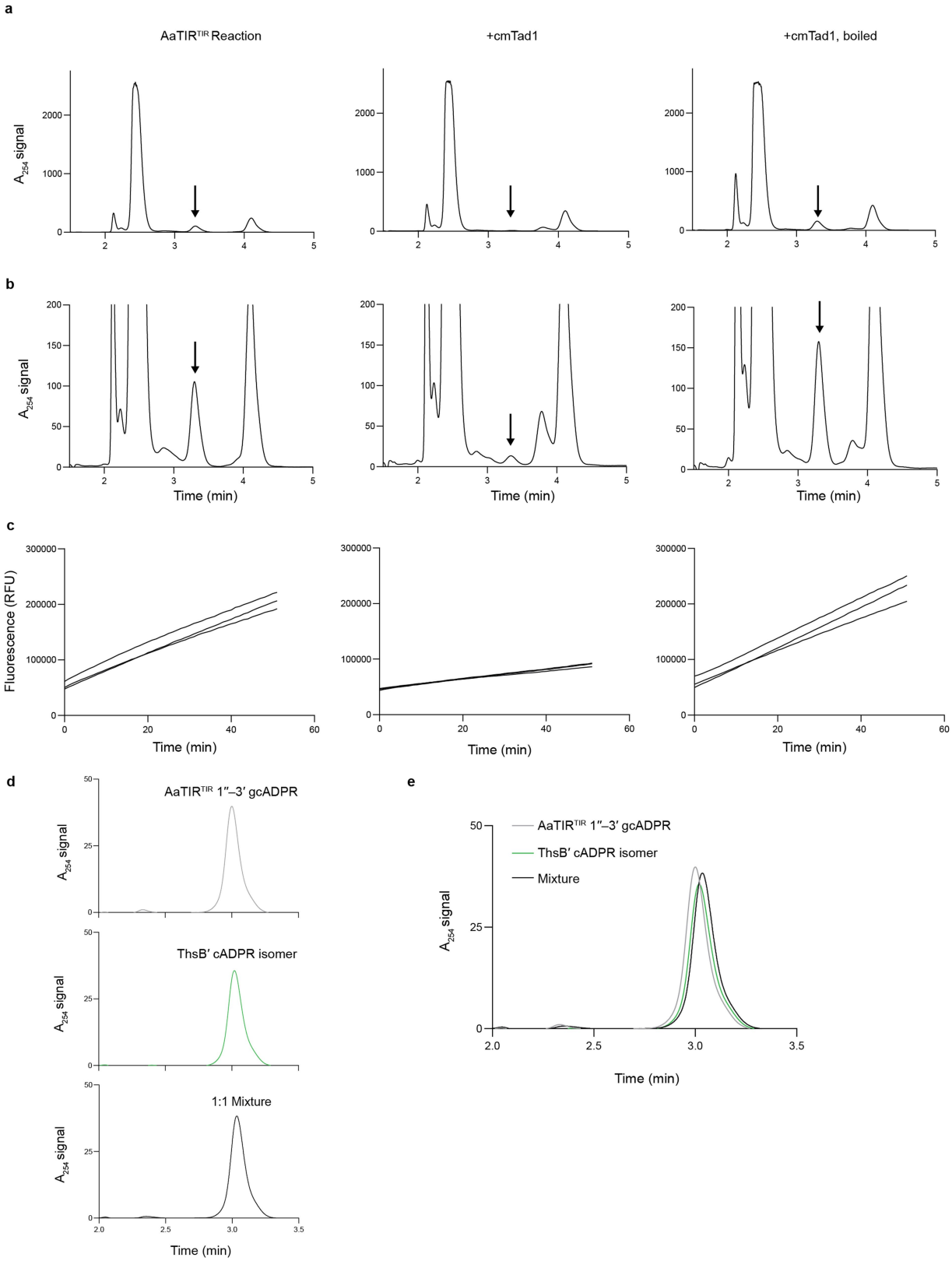

Extended Data Fig. 7 | The Thoeris ThsB-derived cADPR isomer compared to 1″–3′ gcADPR. a, Purified AaTIR^{TIR} was incubated with NAD$^+$, and the reaction products were filtered, treated with buffer, cmTad1, or cmTad1 with subsequent boiling, and analyzed by HPLC. **b**, Y-axis zoom of panel (a). cmTad1 selectively binds, and upon boiling, releases the AaTIR^{TIR} product, 1″–3′ gcADPR. **c**, Filtered reaction products from panel (a) were diluted 1:1000 and tested for activation of ThsA NADase activity. **d**, HPLC analysis of purified ThsB′ cADPR isomer and the fractionated AaTIR^{TIR} reaction shows consistent retention times for 50 μM 1″–3′ gcADPR, 50 μM ThsB′ cADPR isomer, and a 50 μM equimolar mixture of the two, demonstrating that ThsB′ produces 1″–3′ gcADPR. **e**, Overlay of traces from (d).

Extended Data Table 1 | Summary of crystallography data collection, phasing and refinement statistics

	cbTAD1 SeMet **(7UAV)**	cbTAD1–1″–2′ gcADPR **(7UAW)**
Data collection		
Space group	H 3 2	H 3 2
Cell dimensions		
a, *b*, *c* (Å)	155.95, 155.95, 161.45	123.98, 123.98, 112.53
α, β, γ (°)	90.00, 90.00, 120.00	90.00, 90.00, 120.00
Resolution (Å)	48.67–2.20 (2.27–2.20)	48.45–1.72 (1.75–1.72)
R_{pim}	3.3 (79.3)	5.4 (56.6)
$I / \sigma(I)$	15.2 (1.5)	6.8 (1.1)
Completeness (%)	100.0 (100.0)	100.0 (99.4)
Redundancy	41.5 (41.8)	7.7 (3.9)
Refinement		
Resolution (Å)	48.67–2.20	48.45–1.72
No. reflections		
Total	1591383	270425
Unique	38341	35228
Free	2000	2000
R_{work} / R_{free}	20.09 / 24.78	16.53 / 19.79
No. atoms		
Protein	4696 (5 copies)	2006 (2 copies)
Ligand / ion	–	70 (1″–2′ gcADPR)
Water	114	273
B-factors		
Protein	67.55	33.90
Ligand / ion	–	26.91
Water	55.51	44.21
R.m.s. deviations		
Bond lengths (Å)	0.002	0.013
Bond angles (°)	0.400	1.430

All datasets were collected from individual crystals. Values in parentheses represent the highest-resolution shell.

Extended Data Table 2 | Atomic assignment of NMR peaks

Atom	δ (ppm)
1 N	226.43
2 C	153.02
2 H	8.17
3 N	216.29
4 C	149.45
5 C	118.42
6 C	155.75
7 N	235.01
8 C	139.91
8 H	8.68
9 N	167.15
1’ C	84.07
1’ H	6.18
2’ C	75.67
2’ H	4.81
3’ C	72.10
3’ H	4.48
4’ C	85.70
4’ H	4.39
5’ C	65.42
5’Ha	4.15
5’Hb	4.03
1” C	105.51
1” H	5.15
2” C	72.50
2” H	3.44
3” C	69.82
3” H	3.97
4” C	82.32
4” H	4.03
5” C	65.31
5”Ha	4.07
5”Hb	3.92

Multiplets: ^{1}H NMR (600 MHz, D_2O) δ 8.68 (s, 1H), 8.17 (s, 1H), 6.17 (d, *J* = 8.5 Hz, 1H), 5.15 (d, *J* = 4.3 Hz, 1H), 4.81 (dd, *J* = 8.5, 4.6 Hz, 1H), 4.48 (d, *J* = 4.6 Hz, 1H), 4.41 – 4.38 (m, 1H), 4.15 (dd, *J* = 11.3, 5.6 Hz, 1H), 4.09 – 4.05 (m, 1H), 4.05 – 4.00 (m, 2H), 3.98 (t, *J* = 4.6 Hz, 1H), 3.92 (dt, *J* = 11.5, 3.9 Hz, 1H), 3.44 (t, *J* = 4.6 Hz, 1H). ^{13}C NMR (151 MHz, D_2O) δ 155.75, 153.02, 149.45, 139.90, 118.42, 105.51, 85.70 (d, *J* = 9.8 Hz), 84.07, 82.32 (d, *J* = 10.3 Hz), 75.66, 72.50, 72.10, 69.81, 65.42 (d, *J* = 4.5 Hz), 65.31 (d, *J* = 5.0 Hz).

nature portfolio

Corresponding author(s): Azita Leavitt, Erez Yirmiya, Gil Amitai, Allen Lu, Jeremy Garb, Ehud Herbst, Benjamin R. Morehouse, Samuel J. Hobbs, Sadie P. Antine, Zhen-Yu J. Sun, Philip J. Kranzusch, Rotem Sorek

Last updated by author(s): Sep 11, 2022

Reporting Summary

Nature Portfolio wishes to improve the reproducibility of the work that we publish. This form provides structure for consistency and transparency in reporting. For further information on Nature Portfolio policies, see our Editorial Policies and the Editorial Policy Checklist.

Statistics

For all statistical analyses, confirm that the following items are present in the figure legend, table legend, main text, or Methods section.

n/a	Confirmed	
☐	☒	The exact sample size (*n*) for each experimental group/condition, given as a discrete number and unit of measurement
☐	☒	A statement on whether measurements were taken from distinct samples or whether the same sample was measured repeatedly
☐	☒	The statistical test(s) used AND whether they are one- or two-sided *Only common tests should be described solely by name; describe more complex techniques in the Methods section.*
☒	☐	A description of all covariates tested
☒	☐	A description of any assumptions or corrections, such as tests of normality and adjustment for multiple comparisons
☐	☒	A full description of the statistical parameters including central tendency (e.g. means) or other basic estimates (e.g. regression coefficient) AND variation (e.g. standard deviation) or associated estimates of uncertainty (e.g. confidence intervals)
☐	☒	For null hypothesis testing, the test statistic (e.g. *F*, *t*, *r*) with confidence intervals, effect sizes, degrees of freedom and *P* value noted *Give P values as exact values whenever suitable.*
☒	☐	For Bayesian analysis, information on the choice of priors and Markov chain Monte Carlo settings
☒	☐	For hierarchical and complex designs, identification of the appropriate level for tests and full reporting of outcomes
☒	☐	Estimates of effect sizes (e.g. Cohen's *d*, Pearson's *r*), indicating how they were calculated

Our web collection on statistics for biologists contains articles on many of the points above.

Software and code

Policy information about availability of computer code

Data collection	IMG Database October 2017, Metagenomic Gut Virus (MGV) Database, TraceFinder Version 4.1
Data analysis	Cutadapt 2.8, SPAdes 3.14.0, Prodigal 2.6.3, MMseqs2 (release 12-113e3), MAFFT 7.402, IQ-TREE 1.6.5, iTOL24 5, Phenix 1.19.2_4158, Wincoot 0.9.6, SSRL autoXDS, Unicorn (Cytiva) 7, MestReNova 14.3.0, Origin 7, GraphPad Prism 9, PyMOL 2.3.0, Clinker 1.78

For manuscripts utilizing custom algorithms or software that are central to the research but not yet described in published literature, software must be made available to editors and reviewers. We strongly encourage code deposition in a community repository (e.g. GitHub). See the Nature Portfolio guidelines for submitting code & software for further information.

Data

Policy information about availability of data

All manuscripts must include a data availability statement. This statement should provide the following information, where applicable:

- Accession codes, unique identifiers, or web links for publicly available datasets
- A description of any restrictions on data availability
- For clinical datasets or third party data, please ensure that the statement adheres to our policy

Data that support the findings of this study are available within the article and its Supplementary Tables and Supplementary files. IMG/MGV accessions, protein sequences and nucleotide sequences appear in Supplementary Tables 2–4. Coordinates and structure factors of cbTad1 apo, and cbTad1–1''–2' gcADPR have been

deposited in the PDB under the accession codes 7UAV and 7UAW. The genome sequences of phages SBSphiJ1-SBSphiJ7 have been deposited to GenBank under the accession codes OM982668-OM982674, respectively.

Human research participants

Policy information about studies involving human research participants and Sex and Gender in Research.

Reporting on sex and gender	NA
Population characteristics	NA
Recruitment	NA
Ethics oversight	NA

Note that full information on the approval of the study protocol must also be provided in the manuscript.

Field-specific reporting

Please select the one below that is the best fit for your research. If you are not sure, read the appropriate sections before making your selection.

☒ Life sciences ☐ Behavioural & social sciences ☐ Ecological, evolutionary & environmental sciences

For a reference copy of the document with all sections, see nature.com/documents/nr-reporting-summary-flat.pdf

Life sciences study design

All studies must disclose on these points even when the disclosure is negative.

Sample size	Experiments were performed in triplicates without prior sample size calculation (unless mentioned otherwise), as is standard for such experimental designs.
Data exclusions	No data were excluded from the analyses.
Replication	Experiments were performed in triplicates. No failed replications occurred.
Randomization	X-ray crystal structures were refined using a randomly selected set of R-free reflections.
Blinding	Blinding was not required in this study as data were collected using highly quantitative measures over multiple independent replicates.

Reporting for specific materials, systems and methods

We require information from authors about some types of materials, experimental systems and methods used in many studies. Here, indicate whether each material, system or method listed is relevant to your study. If you are not sure if a list item applies to your research, read the appropriate section before selecting a response.

Materials & experimental systems

n/a	Involved in the study
☒	☐ Antibodies
☒	☐ Eukaryotic cell lines
☒	☐ Palaeontology and archaeology
☒	☐ Animals and other organisms
☒	☐ Clinical data
☒	☐ Dual use research of concern

Methods

n/a	Involved in the study
☒	☐ ChIP-seq
☒	☐ Flow cytometry
☒	☐ MRI-based neuroimaging